This is to certify that the
thesis entitled

POOL BOILING HEAT TRANSFER
FROM POROUS-COATED SURFACES IN FC-72:
THE EFFECTS OF SUBCOOLING AND
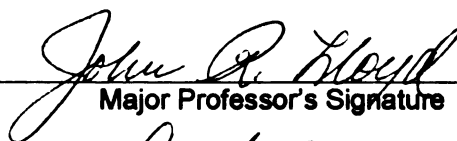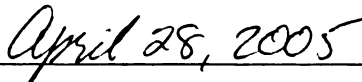NON-BOILING IMMERSION TIME

presented by

KUIYAN XU

has been accepted towards fulfillment
of the requirements for the

M.S.   degree in   Department of Mechanical
Engineering

_____
Major Professor's Signature

April 28, 2005
_____
Date

PLACE IN RETURN BOX to remove this checkout from your record.
TO AVOID FINES return on or before date due.
MAY BE RECALLED with earlier due date if requested.

DATE DUE	DATE DUE	DATE DUE

POOL BOILING HEAT TRANSFER FROM POROUS-COATED SURFACES
IN FC-72: THE EFFECTS OF SUBCOOLING AND
NON-BOILING IMMERSION TIME

By

Kuiyan Xu

A THESIS

Submitted to
Michigan State University
in partial fulfillment of the requirements
for the degree of

MASTER OF SCIENCE

Department of Mechanical Engineering

2005

ABSTRACT

POOL BOILING HEAT TRANSFER FROM POROUS-COATED SURFACES IN FC-72: THE EFFECTS OF SUBCOOLING AND NON-BOILING IMMERSION TIME

By

Kuiyan Xu

The present research is an experimental study of pool boiling behavior of surfaces coated with thin porous layers. The fluid employed is FC-72, a highly-wetting dielectric perfluorocarbon with zero ozone-depletion potential (ODP). This creates the potential for electronic cooling application. Different surfaces, including the super-smooth surface (SSS), the High Flux ™ surface (HFS), and the new electrochemical deposition surface (EDS) were tested, and the test results were compared. Both subcooled and saturated fluid pools were studied. The boiling hysteresis phenomenon was studied for these surfaces under different boiling conditions, which include the fluid bulk temperature and the non-boiling immersion time. Results of the study showed that the porous-coated surface dramatically enhanced the nucleate boiling heat transfer performance. The boiling hysteresis phenomenon is more prominent on porous-coated surfaces than on smooth surfaces, and subcooling can deteriorate this phenomenon.

ACKNOWLEDGEMENTS

I would like to express my gratitude to my advisor, Dr. John R. Lloyd, for providing me the opportunity to perform this research and to pursue my graduate study under his direction. His patience, support and guidance were invaluable to the completion of this work.

In addition, I wish to acknowledge the efforts of my parents for their education and support in my life. They taught me how to face difficulties and never give up.

Most of all I wish to express my particular gratitude to my wife Rong and daughter Heting for their understanding, support and sacrifice all these years. I could not have gone so far without you.

TABLE OF CONTENTS

LIST OF TABLES

LIST OF FIGURES

LIST OF APPENDICES

NOMENCLATURE

a   length (m)

b   width (m)

E   power (W)

h_{fg} latent heat of vaporization (kJ/kg)

L   length (m)

M   mass (kg)

P   pressure (Pa)

q   heat flux (W/m^2)

q''   heat flux (W/m^2)

R   universal gas constant

R   resistance

r   radius (m)

T   temperature (˚C)

ΔT wall superheat (K)

Δt temperature difference (˚C)

U   voltage (V)

Greek Symbols

β   contact angle

γ contact angle

θ conic angle

θ wall superheat

ρ density (kg/m^3)

σ surface tension (N/m)

φ conic angle

Subscripts

b   bulk liquid

cav   cavity

g   residual gas

in   inside

L   local

out   outside

s   saturation

sat   saturation

sub   subcooled

v   vapor

w   boiling surface

CHAPTER 1

INTRODUCTION

Industrial demands for more efficient boilers and evaporators have spurred the development of methods to increase boiling efficiency. Enhancement of nucleate boiling heat transfer has received ever-growing interest in a variety of industries, such as refrigeration, air-conditioning, and chemical process etc. Many different boiling surfaces with enhancement characteristics have been created in the past. These surfaces take a number of forms from simple low integral fins with various fin profiles to more complicated re-entrant cavity type surfaces, such as structured and porous coated surfaces.

In this work the fluid employed is FC-72, a highly-wetting dielectric perfluorocarbon with zero ozone-depletion potential (ODP). This creates the potential for electronic cooling application. Different surfaces, including the super-smooth surface (SSS), the High Flux ^{TM} surface (HFS), and the new electrochemical deposition surface (EDS) were tested, and the test results were compared. A pool boiling facility was designed to perform the experiment. Both subcooled and saturated fluid pools were studied. The boiling hysteresis phenomenon was studied for these surfaces under different boiling conditions, which include the fluid bulk temperature and the non-boiling immersion time of the surface.

1.1 POOL BOILING

Pool boiling refers to a situation in which the bulk liquid is quiescent and its motion near the surface is due to free convection and to mixing induced by bubble growth and detachment. Pool boiling heat transfer can be described with reference to the pool boiling curve, which shows the relationship between the heat flux leaving the heated wall and temperature difference between the heated surface and the surrounding bulk fluid, also known as the wall superheat.

Figure 1.1 shows the boiling curve and boiling regimes for boiling on the outside of a typical plain, smooth tube in water. The curve is divided into four distinct heat transfer regimes: single-phase natural convection, nucleate pool boiling, transition boiling, and film boiling.

As the wall superheat increases from an initial value of zero, the regime is in single-phase natural convection regime until the first vapor bubbles form on the heated wall (Point A in Figure 1.1), which is called the incipience of boiling.

As the heat flux increases to a higher value, point B, the nucleate pool boiling regime has been attained. In this regime the surface is densely populated with vapor bubbles, and most of the heat change is through direct transfer from the surface to the liquid which is in motion at the surface, not through the vapor bubbles rising from the surface.

With the increase of the superheat, a maximum in the heat flux is reached (Point C in Figure 1.1). This point is the peak nucleate heat flux and usually termed as the

critical heat flux.
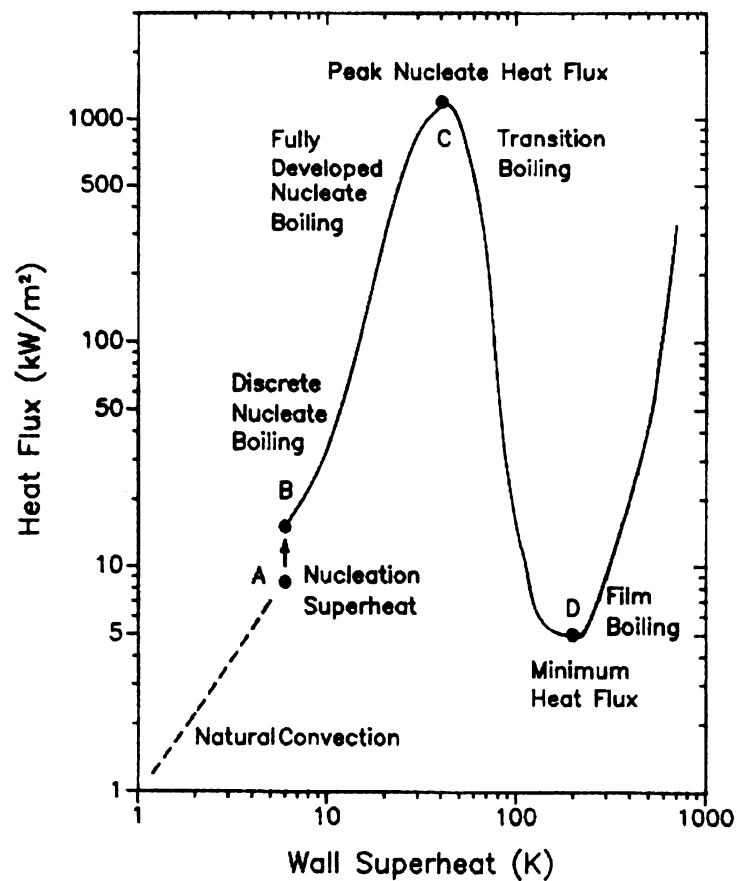
Figure 1.1 Boiling curve and boiling regimes for a plain horizontal tube [42].

After the curve reaches point D, the minimum heat flux point, the regime enters

the film boiling, in which the surface is totally covered by a vapor blanket. In this

regime, heat is transferred from the surface to the liquid via conduction and radiation of

the vapor.

Vapor formation and bubble dynamics in the regime of nucleate boiling, transition

boiling, and film boiling are shown in Figure 1.2. These photographs are from boiling

3

of methanol on a horizontal tube.

1.2 ENHANCED SURFACES

Enhanced surfaces exhibit significantly higher heat transfer than smooth plain surfaces. Thome [42] proposed two important parameters to consider for enhancing boiling heat transfer: boiling nucleation and nucleation site density. Boiling nucleation is the wall superheat required for boiling incipience, and nucleation site density is the number of active boiling sites per unit area of the heated surface. A surface is considered enhanced when either the surface requires a lower wall superheat for boiling incipience, or it can generate a higher number of active nucleation sites than a smooth plain surface.

1.2.1 Machined Surfaces

Machined surfaces are those treated with mechanical methods and contain grooves and cavities which can act as active nucleation site of boiling. One of the earliest surfaces for enhanced boiling performance was a plain surface roughened with emery paper or other abrasives. Corty and Foust [16] used different grades of emery
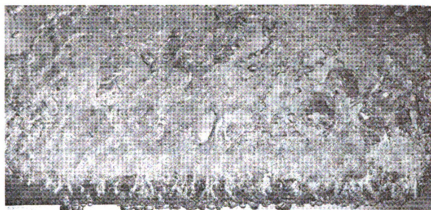
(a)
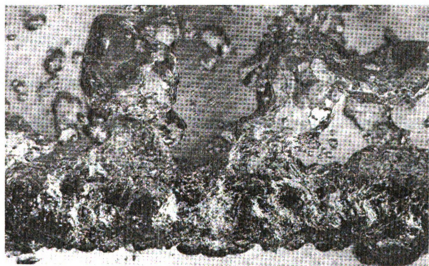
(b)
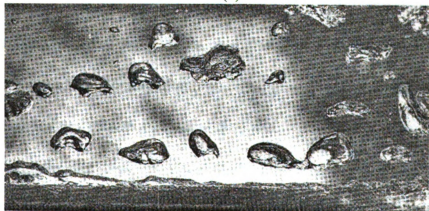
(c)

Figure 1.2 Boiling of methanol on a horizontal tube. (a) Nucleate boiling. (b) Transition boiling. (c) Film boiling. Photographs courtesy of Professor J. W. Westwater, University of Illinois at Urbana-Champaign [21].

paper to produce nickel surfaces with scratches ranging from 0.254 to 25.4 μm across by 0.05 to 0.635 μm deep. They demonstrated that increasing roughness alone has limitations on enhancement of the boiling process. Berenson [4, 5] used a combination of mechanical roughening and oxidation to treat the surface. He found that the slope of the boiling curve is higher for the roughened surfaces than for the mirror-finished surface, and that variation of surface roughness can hardly affect the critical heat flux.

The first patent for an extended surface on the purpose of heat transfer enhancement was obtained by Still [40]. He applied this in the forced convection to air on the outside of a tube. In 1960, Webber [45] successfully applied the finned tube reboiler in a refinery light end unit. These studies demonstrated the viability of finned surfaces in industrial applications. Myers and Katz [31] demonstrated that the fins can not only increase the surface area but also change the boiling process to enhance performance.

Chien and Webb [10] proposed two key geometric characteristics of the surfaces are subsurface tunnels and surface pores or fin gaps. They believe that the important dimensional parameters include the following: tunnel pitch, tunnel height, tunnel width, tunnel base radius, tunnel shape, pore diameter, and pore pitch. Chien and Webb [10, 11, and 13] performed a series studies using R-11, R-22, R-123, and R-134a as the working fluids for an extensive variety of parameter combinations. They found that: (1) the boiling heat transfer rate decreases as the tunnel height is reduced; (2) sharp tunnel corners provide a greater enhancement; and (3) the boiling coefficient is strongly

influenced by pore size at a given heat flux.

Ramaswamy et al [35] investigated an enhanced surface consisting of a stacked network of interconnecting channels which makes it highly porous. They studied the effect of varying the pore size, pitch and height on the boiling performance with fluorocarbon FC-72 as the working fluid. They found that a larger pore and a smaller pitch resulted in higher heat dissipation at all heat fluxes. The heat dissipation increases with an increase in the pore size (for the same pore pitch). In the range of pore sizes tested (90–320 μm), the largest pore size resulted in maximum heat dissipation. It was found that the effect of pore pitch on heat transfer performance was more significant than the pore size.

Jiang et al [22] investigated the microfilm evaporation and two-phase flow inside the microstructure of a machined porous surface and developed a new microscale heat transfer model for boiling heat transfer on porous surfaces. They used R11, R22, R134a, and water as the working fluids and determined the optimum microstructure for the given conditions. Their results demonstrated that the heat transfer performance of porous surfaces is augmented by enhancing the evaporation of the thin liquid films inside the microchannels. They believe that the surface tension and evaporation of the working fluids are the two most important parameters. For boiling in fluids with large surface tensions, it is better to choose larger pore diameter and smaller space between two pores. They also found that sharp channel corner angles, rough surfaces and crossed channels can bring larger heat transfer area inside the channels.

1.2.2 Porous-coated Surfaces

Porous-coated surfaces are widely used in heat exchangers, heat pipes, and electronic cooling. In these surfaces, an irregular matrix of potential nucleation sites is formed by means of poor welding, sintering or brazing of particles, electrolytic deposition, flame spraying, bonding of particles by plating, galvanizing, plasma spraying of a polymer, or metallic coating of a foam substrate [8].

Milton got his patent for a porous sintered metallic coating in 1968 [30]. After further improvement, he developed the commercial surface-High Flux ™. This surface contains many irregular cavities similar to those of coral [23]. The particles are sintered onto the surface and form randomly shaped cavity openings that are approximately 0.04 to 0.13 mm in diameter. The thickness of the porous coating is approximately 0.645 mm. The porosity of the matrix is 45%. Since the High Flux ™ surface can provide superior boiling heat transfer performance, it is often used as a benchmark for evaluating boiling performance of other porous coated surfaces [1].

Thome [42] proposed that the key parameters for porous-coated surfaces include particle size, layer thickness, particle material, and porosity. But it is difficult to determine an optimal combination of these parameters to maximize boiling performance.

With FC-72 as the working fluid, Chang and You [9] investigated particle size effects on the boiling performances of micro-porous enhanced surfaces using five different sizes of diamond particles. They compared the coating thicknesses with the

superheated layer thickness and classified the coatings into two groups: 'micro-porous' and 'porous' coatings (Figure 1.3).   The micro-porous surfaces correspond to the
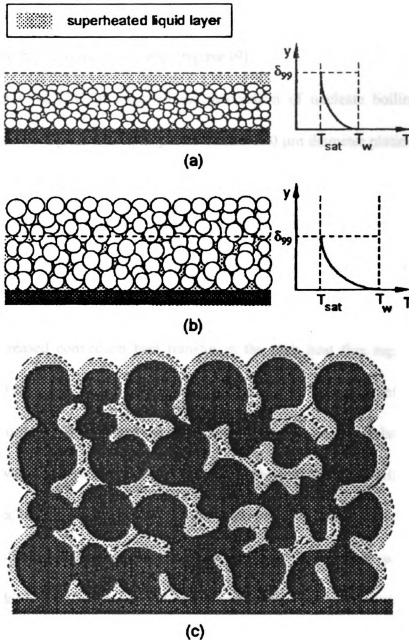
Figure 1.3 Theoretical models of (a) Micro-porous. (b) Porous non-conducting coated surfaces. (c) Porous conducting surfaces [9].

coatings with thickness ≤ 100 μm and the porous coatings have a thickness > 100 μm.

The superheated layer thickness, δ_{99}, is calculated using one-dimensional transient heat conduction. The micro-porous coatings show different characteristics of boiling performance compared to porous coatings in incipient superheat, nucleate boiling and CHF. A significant decrease of incipience superheat and an increase of CHF was observed for the micro-porous surface regime [9].

Kim et al [24] investigated the mechanism of nucleate boiling heat transfer enhancement from plain and microporous coated 390 μm diameter platinum wires. The materials they used for the microporous coated wire is the dielectric DOM (8-12 μm synthetic Diamond particles/Omegabond 101 epoxy binder/Methyl-ethyl-keytone carrier). Their results showed that the microporous coatings augment nucleate boiling performance through increased latent heat transfer in the low heat flux region and through increased convection heat transfer in the high heat flux region. The results showed that the CHF for the microporous coated surface is significantly enhanced over the plain surface. They believed that this is due to decreased latent heat transfer (decreased vapor generation rate) and/or increased hydrodynamic stability from increased vapor inertia, both of which are a direct result of increased nucleation site density.

Cieslinski [14] performed series experiments of heat transfer with distilled water as the working fluid. He used stainless steel tubes of different diameters and flat horizontal surfaces ranging from a smooth lapped finish through sandblasted surfaces, to porous coated surfaces. Various methods of variation of surfaces, such as electrolytic treatment, plasma spraying, gas-flame spraying and modified gas-flame spraying were

10

employed to form metal coatings. The results showed that the main parameters of the porous coating that influence boiling heat transfer are thickness and porosity. It is not affected by the methods of fabrication, providing the contact between the porous matrix and the substrate is good.

1.3 PARAMETRIC EFFECTS

Pool boiling heat transfer performance can be affected by many parameters, such as system pressure, subcooling, and electric field imposed on the working fluid. Some of these parameters can change the boiling performance dramatically.

1.3.1 Pressure

Thome [42] reported that the boiling curves of plain surfaces should move to the left with increasing pressure. Rainey et al [33] investigated the effect of pressure, subcooling, and dissolved gas on pool boiling heat transfer from 1 cm^2 plain and microporous flat copper blocks immersed in FC-72. They found that the incipient superheat increases with decreasing pressure for both microporous and plain surfaces. The difference in the nucleate boiling performance between the plain and microporous surfaces appears to decrease with increased pressure. The CHF values also show a significant increasing trend with increased system pressure.

Nakayama et al [32] investigated the influence of system pressure on saturated pool nucleate boiling heat transfer with R-11 as the working fluid. They found that at

11

smaller superheats, the higher the system pressure, the higher heat fluxes are sustained at reduced wall superheat.

Zhang et al [46] performed experiments on pool boiling heat transfer from a circumference-interrupted T-finned (CIT) tube and a Thermoexcel-E type tube at system pressures ranging from 1 to 6 bar with ethyl alcohol and R-113 as the working fluids. They demonstrated that with the increasing system pressure, the boiling heat transfer coefficient increases at first, but the improvement is smaller for higher pressures. There exists an optimal system pressure beyond which the boiling performance tends to diminish.

1.3.2 Subcooling

The term surface subcooling here means the temperature difference between saturation temperature of the working fluid and the surface. According to Thome [42], the boiling curve moves to the right as the subcooling increases. Even small levels of subcooling can dramatically affect the heat transfer process and substantially reduce the boiling heat transfer coefficient.

Bajorek [3] investigated the effect of subcooling on boiling on a low-finned copper tube. He obtained data for water, ethanol, and several mixtures at 101 kPa for subcooling ranging from 0 – 40 K. He found that the largest drop in the heat transfer coefficient occurred in the first 10 K of subcooling, where boiling performance was reduced by 40% to 50%.

Rainey et al [34] found the most prominent effect of subcooling on boiling was that regardless the subcooling level, the fully developed nucleate boiling curves collapse onto a single line. They believe that as subcooling increases, the bubble departure diameters and frequencies decrease which reduces the amount of heat transferred through latent heat and microconvection. The increased subcooling also decreases the superheated liquid layer thickness which increases natural convection and Marongoni convection heat transfer. These combined effects result in relative insensitivity of the nucleate boiling curve to liquid subcooling.

Demiray et al [17] measured the heat transfer under nucleating bubbles using a microheater array with different subcooling. They found that the individual bubble departure diameter and energy transfer were larger with low subcooling. But as the subcooling increases, the bubble departure frequency increases which results in higher overall heat transfer.

1.3.3 Electric Field

Leontiev et al [26] investigated the effect of an electric field on the boiling of liquid nitrogen. They believed that an external electric field can cause an additional surface force directed into the gas phase and essentially influences the nucleation and bubble dynamics with a dielectric liquid as working fluid. Both uniform and non-uniform electric fields were applied on horizontal smooth and corrugated surfaces. The results showed that uniform electric field with an intensity of up to 10^7 V/m had no

essential influence on the initial part of the boiling curve of the smooth surface. The non-uniform electric field, created by a metallic pin attached to the test surface, reduced the incipience superheat of both the smooth and corrugated surfaces as compared to the results with the uniform electric field.

Vorob'ev et al [44] found that the presence of an external electric field always stimulates vapor bubble formation in superheated liquids. The uniform and non-uniform electric fields initiate both condensation of superheated vapor and boiling of superheated liquid. Provided that the field intensity exceeds some threshold value, the vapor condensation would be intensified with the presence of an external electric field, regardless it is uniform or not. But for the non-uniform field, this threshold value is smaller.

Snyder et al. [39] performed an experiment to produce a dielectrophoretic (DEP) force over the length of a horizontal platinum wire heater. They concluded that the overall boiling heat transfer coefficient in the presence of an electric field can be modeled as the summation of a heat transfer coefficient due to bubble dynamics and a heat transfer coefficient due to electroconvection. In terms of the relationship between the bubble dynamics and the heat transfer, they believed that the effect of a variable DEP force is similar to the effect of a variable buoyancy force. The heat transfer in the presence of an electric field will be enhanced if the effective gravity acts to hold the vapor bubbles near the heated surface, while at the same time permitting access of the liquid to the surface in order to prevent dryout.

1.4 NUCLEATE BOILING MECHANISMS

1.4.1 Boiling on Plain Surfaces

Thome [42] states that a surface appearing to be smooth is actually covered with small cavities of various sizes, shapes, and depths (Figure 1.4). Clark et al [15] have demonstrated that boiling nucleation from a smooth surface occurs at microscopic imperfections in the surface.

Machined Surface

Trapped Vapor Nuclei
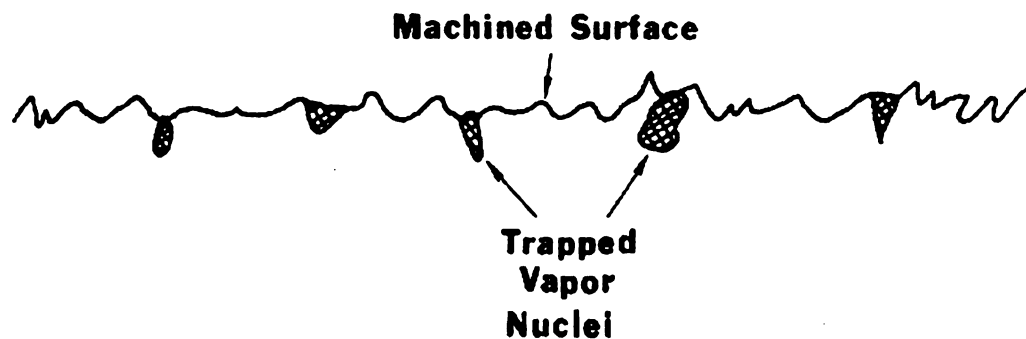
Figure 1.4 Magnified cross-section of a plain, smooth metallic surface [42]

These cavities are on the order of 0.1-10 μm in diameter and act as nucleation sites due to their ability to trap vapor [37]. The trapped vapor grows into a bubble and detaches as the surface is heated. Once the bubble departs from the surface, a liquid film again covers the cavity where some vapor remains trapped. This remaining trapped vapor will act as an embryo for the next bubble.

Bankoff [4] and Griffith and Wallis [18] developed the criteria for a stable vapor trapping conical cavity. It is based on the contact angle, γ, and the cavity cone angle, θ, as shown in Figure 1.5 as

$$\theta < \gamma < 90°$$ (1.1)

When θ and γ satisfy this condition, the incipient superheat is calculated from the Laplace and the Clausius-Clapeyron equations, to get

$$\Delta t = \frac{2\sigma T_{sat}}{\rho_v h_{fg} r_c}$$ (1.2)

where Δt is the temperature difference between the trapped vapor temperature and the distant liquid temperature, σ is the liquid surface tension, T_{sat} is the distant fluid saturation temperature, h_{fg} is the latent heat of vaporization, ρ_v is the density of the vapor, and r_{cav} is the radius of the nucleation site. For such low contact angle liquids as FC-72, Equation 1.1 will be valid only for very steep walled conical cavities. If this criterion is met, Equation 1.2 predicts a minimum incipient superheat of only 1.8K for FC-72 [28].
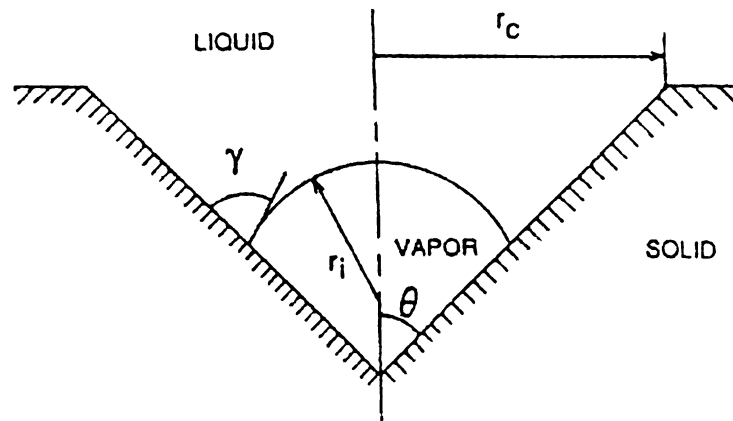
Figure 1.5 Cavity and bubble geometry [29].

16

Hsu and Graham [19] summarized the heat transfer mechanisms responsible for heat transfer in nucleate pool boiling on plain, smooth surfaces as follows (see Figure 1.6) :
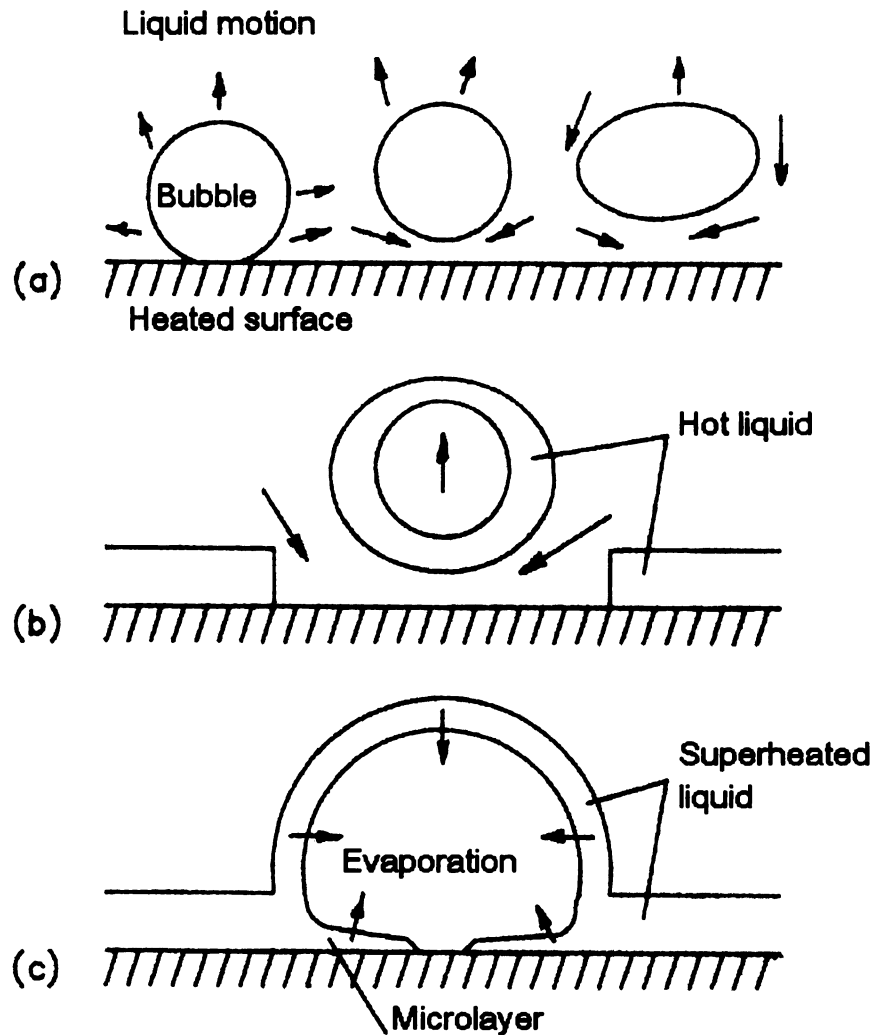
Figure 1.6 Nucleate boiling mechanisms. (a) Bubble agitation, (b) Vapor-liquid exchange, (c) Evaporation [19].

1. Bubble agitation (Figure 1.6 a):   Improved liquid-phase convection results from the motion imparted to the liquid from the growth and departure of vapor bubbles. The natural convection process has been transformed into a "forced" convection process.

Heat is transferred from the surface by the superheated liquid.

2. Vapor-liquid exchange (Figure 1.6 b):   Convection to the liquid is enhanced by the quenching of the heated wall by fresh liquid rushing in after the leaving of a vapor bubble.   The thermal boundary layer covering the bubble and the adjacent wall is continuously removed.

3. Evaporation (Figure 1.6 c):   Vapor bubbles grow by virtue of the heat conducted into the liquid from the heated wall and then to the bubble surface, where phase change happens.   Vaporization occurs from (1) a liquid microlayer trapped between the heated wall and the bottom of a rapidly growing bubble and (2) the original thermal boundary layer covering the top of the bubble.

The actual boiling process is a combination of these three heat transfer mechanisms.

1.4.2 Boiling on Porous Coated Surfaces

Bergles and Chyu [8] postulate the mechanisms of boiling from porous coatings. Consider nucleation in the porous matrix shown in Figure 1.7.   If the matrix material is poorly wetted, vapor or vapor plus noncondensable gas will be retained in the interstitial space when the temperature is reduced below the saturation temperature.   Alternately, if the liquid has more wetting ability, re-entrant and double re-entrant cavities are required to permit stable dropwise formation so that the cavities are not filled with subcooled liquid.   In any case, the matrix increases the probability that nucleation sites are

available which will remain active for repeated cycles of heating and cooling.

Griffith and Wallis [18] demonstrated that the geometry of the micro-cavity containing trapped vapor is important to the bubble nucleation process. They found the re-entrant type of micro-cavities were stable, easily activated boiling sites. Benjamin and Westwater [5] reported the construction of an artificial re-entrant cavity with a mouth diameter of 102μm, which was described to be stable, remaining active down to low wall superheats for boiling mixture of water and ethylene glycol.
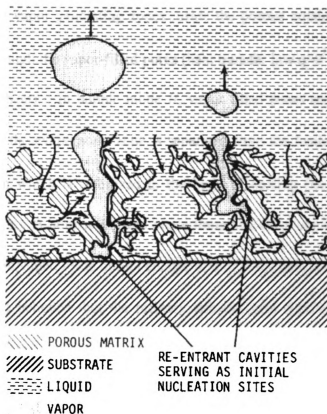
Figure 1.7 Conceptual model of boiling in a porous matrix of sintered metallic particles [8].

Since then, porous metallic coatings have received considerable attention. Formed by bonding metal particles with diameters ranging from 44 to 1000μm to a base surface (coating thickness ranges from 250 to 2000μm), porous metallic coatings have demonstrated to greatly enhance nucleate boiling heat transfer performance.

Andrianov et al [2] believed that porous coatings essentially transform heat transfer laws at bulk boiling. They proposed that there were two possible modes of boiling corresponding to the bubble mechanism of the vapor departure from the outer surface of the coating, whereas there was only one mode on the smooth surface. In bubble mode I, the vapor generating zones inside the porous coating are not connected with each other through the vapor-filled pores (heat transfer law $q{\sim}\theta^n$ corresponds to $n{\neq}1$, θ is the wall superheat). In bubble mode II, vapor filled pores are connected over the whole system, and the evaporation zone is separated from the heated surfaces by a thin layer of vapor film which is stabilized in the body of coating (heat transfer law $q{\sim}\theta^n$ corresponds to $n{=}1$). A nonequilibrium phase transition from one bubble boiling mode to the other is accompanied by an abrupt change of θ or a discontinuity in derivatives.

Thome [43] believed that the primary enhancement mechanisms for re-entrant type enhanced surfaces were: enhanced nucleation from the larger embryonic bubbles, increased thin film evaporation due to the large internal area of the porous structure, and two-phase convection within the porous structure.

1.5 BOILING HYSTERESIS

1.5.1 Boiling Hysteresis Characteristics

Research on the boiling hysteresis phenomenon can be traced back to the 1950s, when Corty and Foust [16] found that the immediate past history of the boiling surface had a pronounced effect on the superheat required for boiling incipience, which was far beyond that required in normal boiling conditions. This is defined as temperature overshoot (TOS), which means the surface temperature is highly superheated preceding the transition from the natural convection state to the nucleate boiling state [38].

Boiling hysteresis can be defined as the discrepancy between the boiling curves obtained by increasing and then decreasing the applied heat flux. For the boiling hysteresis to exist in the boiling developing process, Shi et al [38] termed it as Temperature Deviation (TD) hysteresis. The two kinds of boiling hysteresis phenomena, TOS hysteresis and TD hysteresis, are generalized in Figure 1.8.

Porous-coated surfaces have proven to be an efficient method to increase the performance of boiling heat transfer. But experiments by Bergles [8] and Marto [28] have demonstrated that boiling hysteresis phenomenon is more prominent on porous-coated surfaces than on smooth surfaces.

It is obvious that the boiling hysteresis may jeopardize cooling process of high-power density components. This will restrict the application of pool boiling cooling in the industrial fields.

21
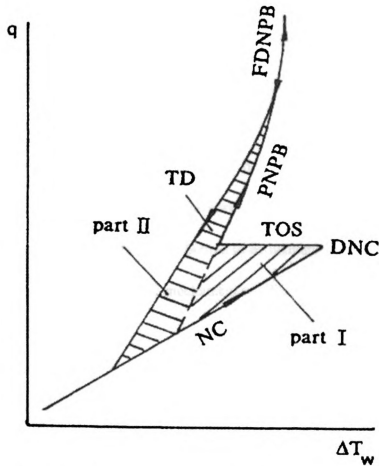
Figure 1.8 Characteristics curves of nucleate pool boiling hysteresis:
FDNPB-fully-developed nucleate pool boiling; PNPB-partial nucleate pool boiling;
DNC-departure from natural convection; NC-natural convection [38].

1.5.2 Boiling Hysteresis Mechanisms

The nucleation of vapor bubbles from embryonic vapor/gas pockets in microcavities on the heated surface has been proven to account for boiling incipience and much of the ebullient heat transfer from metallic surfaces to the boiling fluids [36]. If the surfaces are immersed in the liquid with high wetting characteristics, a large percentage of the cavities would be filled by the liquid. The cavities which trapped

some residual gases would function as the first nucleation sites.

Shi et al [38] analyzed the boiling hysteresis mechanisms. Consider an embryonic bubble with a radius of r_c growing out from a conical cavity. Inside the bubble there may include some noncondensable gases. To achieve mechanically stable of the bubble, the internal pressure of the bubble must exceed the external or the local pressure by an amount proportional to the surface tension dividing by the radius of curvature at the interface. Assuming the bubble to be hemispherical and considering the presence of the initial residual gas, the mechanical equilibrium for this embryonic bubble is:

$$P_v + P_g - P_L = \frac{2\sigma}{r_c} \tag{1.3}$$

where P_v and P_g are the vapor partial pressure and initial partial pressure of the residual gas in the bubble respectively. P_L is the external or local ambient pressure.

From the thermodynamic nucleation theory, the liquid superheat needed to sustain the growth of this embryonic bubble should be

$$\Delta T_{wl} = T_{wl} - T_s = \frac{T_s}{\rho_v h_{fg}} \left(\frac{2\sigma}{cr_c} - P_g \right) \tag{1.4}$$

where c is a constant related to the thermal layer thickness surrounding the bubble. Assuming the residual gas is an ideal gas, so

$$P_g = \frac{3m_g R T_v}{4\pi r_c^3} \tag{1.5}$$

where m_g is the initial mass of residual gas in the cavity. Equation 1.1.2 can then be

expressed as

$$\Delta T_{w1} = \frac{T_s}{\rho_v h_{fg}} \left(\frac{2\sigma}{cr_c} - \frac{3m_g RT_v}{4\pi r_c^3} \right)$$
(1.6)

TOS Hysteresis

TOS hysteresis occurs at the incipience of the boiling process. The first bubbles generate from the cavities in which a small amount of residual gas preexisted. The liquid superheat needed for the first bubble generation can be predicted by equation 1.6. After the first bubbles leave the surface, more residual gas (vapor) will be trapped in these cavities. The liquid superheat needed for further bubble growth is

$$\Delta T_{w2} = \frac{T_s}{\rho_v h_{fg}} \left(\frac{2\sigma}{cr_c} - \frac{3m_{gc} RT_v}{4\pi r_c^3} \right)$$
(1.7)

where m_{gc} is an equivalent mass of the new residual gas-vapor mixture in the cavities. ΔT_{w2} is the normal surface superheat under the given heat flux. Because $m_{gc} > m_g$, then $\Delta T_{w2} < \Delta T_{w1}$. This is why hysteresis will occur at the boiling incipience. The temperature overshoot can be expressed by the following equation:

$$\Delta T_{TOS} = \Delta T_{w2} - \Delta T_{w1} = \frac{3T_s T_v R}{4\pi r_c^3 \rho_v h_{fg}} \left(m_{gc} - m_g \right)$$
(1.8)

From Equation 1.8 it can be seen that the larger the mass of residual gas (vapor) trapped in the cavities, the smaller the temperature overshoot will have at the boiling

incipience.   When $m_{gc}= m_g$, there will be no occurrence of temperature overshoot at all.

TD Hysteresis

Shi et al [38] interpreted the occurrence of the TD hysteresis with the vapor propagation after the incipience of boiling.   As shown in Figure 1.9, the growth of the first bubbles may activate the neighboring cavities which retained less or no residual gas at a lower wall superheat.   With the bubble interface spreading along the surface, the vapor front would enter the neighboring cavity providing the liquid contact angle $\beta >$ (π-φ).   Then the neighboring cavity would be filled with gas (vapor) and be activated (Figure 1.9 a).   In another case, if $\beta <$ (π-φ), which means either the conical angle of the cavity φ is small, or the contact angle of the fluid β is small (Figure 1.9 b), the cavity might initially have a small amount gas in it and not be activated at the initial wall superheat.   If the first growing bubble covers this cavity, the liquid inside the cavity would be separated from the bulk liquid and becomes locally highly superheated by the heated wall.   So the small embryonic bubble would grow because of liquid evaporation and be activated in the next bubble generation.

25
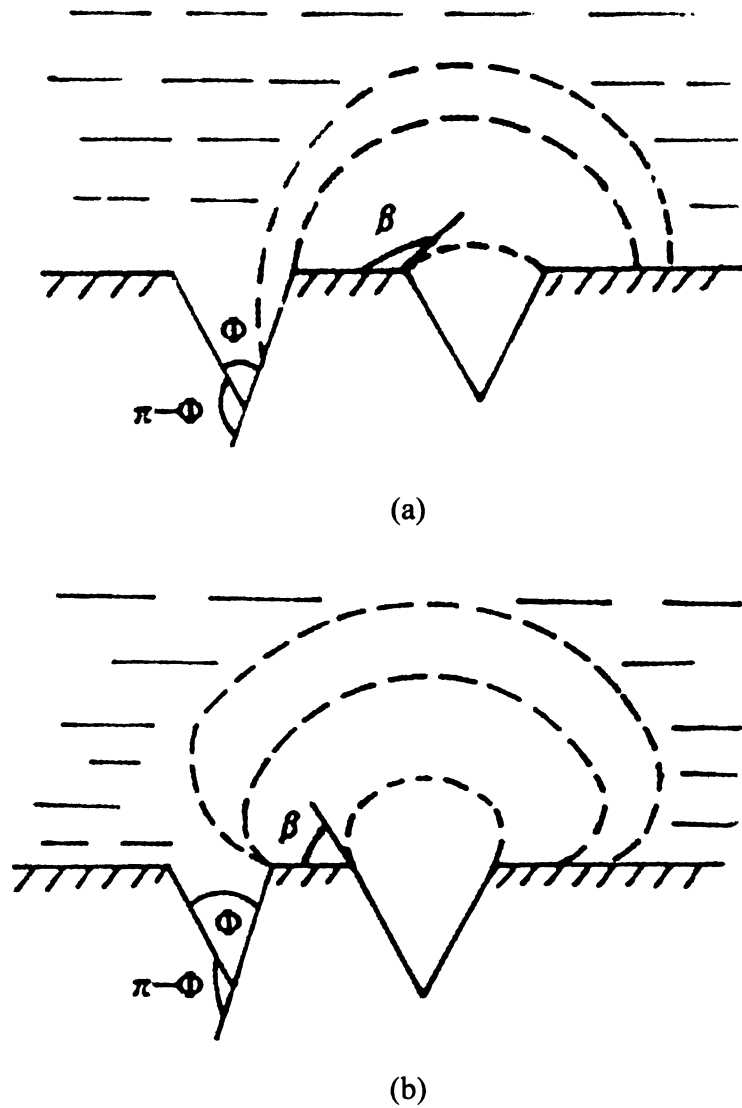
Figure 1.9 Activation of neighboring cavities [38].

After the fully developed nucleate boiling is reached, if the heat flux is then decreased, the cavities which were not activated in increasing heat flux are now active. From equation 1.7 it can be found they need lower wall superheat. So the boiling is augmented compared with the increasing process and causes the deviation of boiling curves, which is termed as the TD hysteresis.

Bergles and Chyu [8] explained the large scale boiling curve hysteresis for High Flux [TM] surfaces with the flooding of the porous matrix with liquid, which resulted only relatively small sites are available for nucleation. They believed that for a specific surface, the contact angle of the working fluid would strongly influence the extent of temperature overshoot.

Tehver et al [41] investigated the relation between the effectiveness of heat transfer and structural parameters of a plasma-sprayed coating with F-113 as the working fluid. They tested different coatings such as aluminum, bronze, copper and corundum. The great variety hysteresis phenomena they observed suggest there are two main factors: (1) the boiling incipience conditions determined by the availability of active center embryos and (2) the structure of a porous material characterized by non-uniform pore cross sections for liquid and vapor flows. The joint influence of these two factors, which depend on the wetting contact angle and the experimental conditions, results in a great variety of boiling curves for porous surfaces.

This work will investigate the influence of subcooling and non-boiling immersion time of test surfaces to the nucleate pool boiling performance. A new porous coating is studied in this work using highly wetting fluid FC-72. Subcooled pool boiling data in FC-72 and water are compared and discussed to demonstrate the effect of contact angle between the fluid and the surface for the two fluids.

CHAPTER 2

EXPERIMENTAL APPARATUS AND PROCEDURE

2.1 EXPERIMENTAL APPARATUS

2.1.1 Test Facility

The experimental setup for this study is shown in Figure 2.1. The test fluid, FC-72, is a highly-wetting dielectric perfluorocarbon produced by the Industrial Chemical Products Division of 3M. The test liquid was contained within a 3500 ml Pyrex beaker that was submerged in a 40cm×20cm×27cm vessel. This vessel served as a constant temperature water bath. A Fisher 90 Refrigerated Bath was used to heat the water to 56°C for the saturated tests, or 51°C for the 5 K subcooled test. An insulation layer was applied to prevent heat losses of the water bath. The tests were conducted at atmospheric pressure. An external, water-cooled condenser made by copper tube was used during the test to prevent loss of the testing liquid.

A copper-constantan (Type T) thermocouple was placed within the test vessel to measure the bulk test liquid temperature. The test section was mounted horizontally and immersed in the test liquid.

The test section used in this research consisted of the test surface, the 25mm×45mm×45mm copper block with two embedded T-type thermocouples and a cartridge heater. Since copper has very high thermal conductivity, it is an ideal heat transfer material.
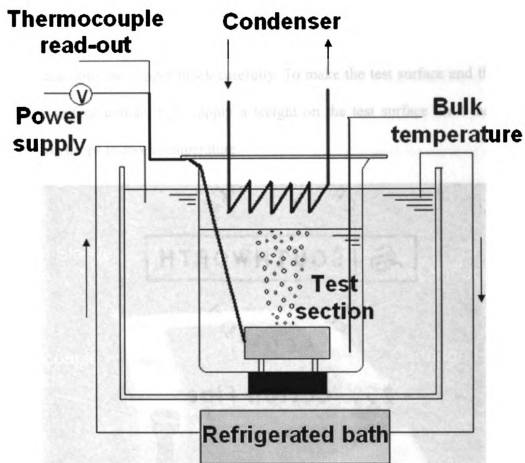
Figure 2.1 Schematic of experimental setup.

The copper block was covered by Teflon sleeves on all sides except the top one. Silicon sealant was applied between the copper block and the Teflon sleeves to prevent liquids from entering the inside of the test section. Figure 2.2 shows the structure of the test section with the front Teflon sleeve removed.

Test surfaces are soldered on the top surface of the copper block. When

soldering the test surface, first cut the solder into 1 cm pieces. Second, turn on the power to the cartridge heater until the thermal couple reading reaches 140 ˚C. Then apply the solder to the upper surface of the copper block. After the solder is melted, put the test surface onto the copper block carefully. To make the test surface and the copper block upper surface contact tight, apply a weight on the test surface until the thermal couple reading drops to room temperature.
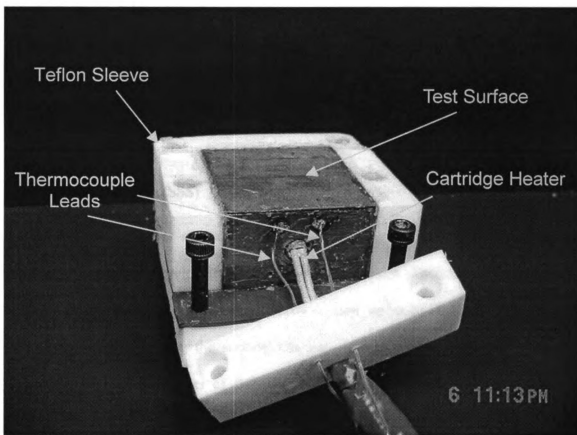
Figure 2.2 Heat transfer test section with front Teflon sleeve removed.

To measure the surface temperature of the test specimen, two copper-constantan thermocouples (30 gauge, 0.075cm in diameter) were inserted and soldered into two

holes drilled in the copper block (1-mm in diameter, 5-mm in depth).

The thermocouples were connected to an OMEGA HH23 Microprocessor Thermometer. The test surfaces were heated by the 0.635cm diameter by 3.81cm long 125-Watt Chromalox model CIR-1015 cartridge heater. The heater was first coated with Chromalox Boron Nitride Lubricoat and then inserted into a pre-drilled hole in the copper block. A Powerstat Variable Autotransformer was used to control the input of the power into the heater and the value of the voltage was displayed in a Wavetek 15XL multimeter.

2.1.2 Test Surfaces

Super Smooth Surface (SSS)

The copper super smooth surface was prepared by Ngai [33] following the preparation procedure developed by Aitcheson [1]. At first, distilled water was used to wash off the dirt on the copper surface. Then acetone was used to dissolve the possible oil and grease. After that, the surface was wiped clean with a soft cloth before the polishing process. Sandpaper of different grits and diamond polishing compounds of different grit sizes were used successively to process the surface. The copper surface was first sanded 50 times in one direction using 320-grit sandpaper, then cleaned and sanded 50 times in the direction perpendicular to the previous sanding direction. Sandpapers of 400-grit, 600-grit, 1200-grit and 4000-grit, diamond-polishing compounds of 6 micron, 3 micron, 1 micron and 0.25 micron were used progressively to remove the scratches from the previous grit and get a smooth mirror-like surface.

Electrochemical Deposition Surface (EDS)

The electrochemical deposition surface (EDS) was created by Nicole Aitcheson [1] using the procedure developed by Lloyd [27]. Figure 2.3 shows the experimental set-up used for electrochemical deposition. The electrolyte solution was an aqueous solution of 1.5 molar reagent grade sulfuric acid (H_2SO_4) and 0.05 molar copper sulfate ($CuSO_4$). The copper ions of the $CuSO_4$ served as the transferred species of ions and the H_2SO_4 was the supporting electrolyte.
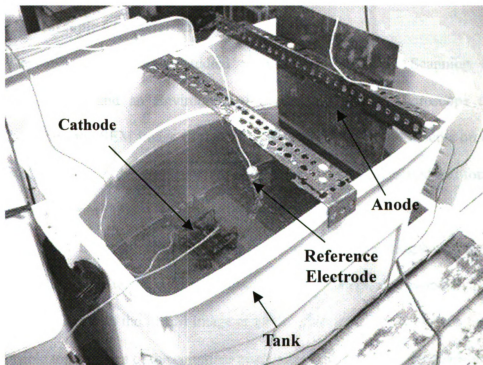
Figure 2.3 Electrochemical deposition experimental set-up [1].

The anode and cathode were made from thick copper sheets with dimensions of 54.3 cm×30.5 cm×0.32 cm and 6.0 cm×7.5 cm×0.32 cm respectively. The anode surface area was 34 times larger than the surface area of the cathode to insure that the electrode reaction would be controlled by the cathode. A 14 gauge copper wire was inserted into a

polyethylene test tube with a capillary hole drilled in the bottom to serve as the reference electrode. The cathode was the test surface for electrochemical deposition.

High Flux ^{TM} Surface (HFS)

The High Flux ^{TM} surface (HFS) was acquired from the commercially available High Flux ^{TM} tube by UOP. First, one side of the tube was cut along the axial direction, and then it was flattened carefully with a plastic hammer. After that, it was cut into pieces of 4.5cm×4.5cm to be tested.

Surface Microscopic Characteristics

The test surfaces were studied with a high-resolution Scanning Electron Microscope (SEM) and an Environmental Scanning Electron Microscope (ESEM). Figure 2.4 shows the SEM image of the SSS. By taking 50 measurements on different locations of the surface, the average width of the scratches was calculated and found to be approximately 200nm [33].

The SEM image of HFS is shown in Figure 2.5. The lengths of the surface structure vary in a wide range, with a maximum length of 48 μm approximately [33].

Figure 2.6 shows the ESEM image of EDS. The particle-like surface formations are the visible top surfaces of the columnar protrusions. Aitcheson [1] determined the
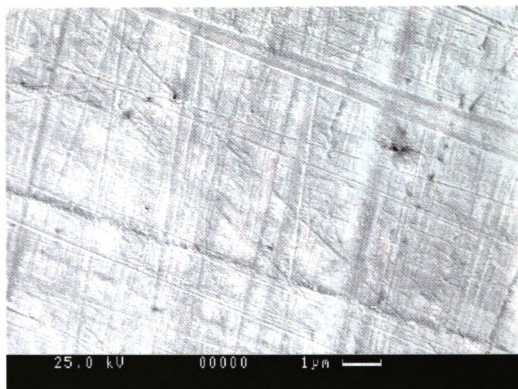
Figure 2.4 SEM image of the SSS [33].
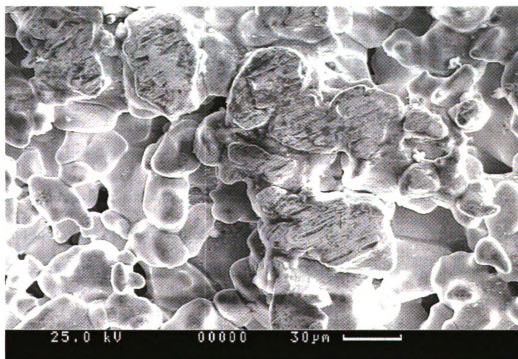
Figure 2.5 SEM image of the HFS [33].
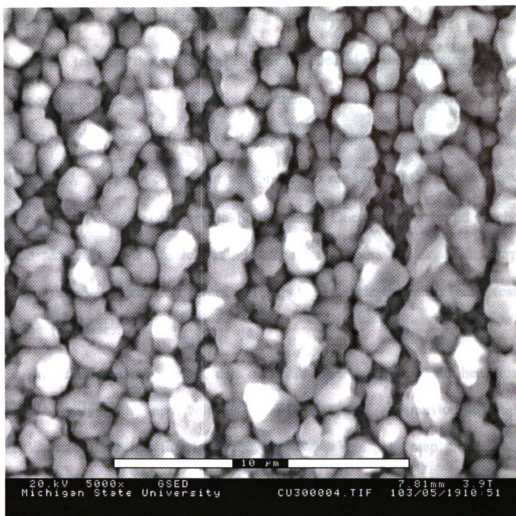
Figure 2.6 ESEM image of the EDS [1].

average column-face sizes using the reference scale provided on the ESEM image. Column-face sizes were measured at 20 different locations and were then taken an average. The average column-face sizes of the EDS ranged from 0.7 μm to 1.5μm.

2.2 EXPERIMENTAL PROCEDURE

Before the test, the surfaces were immersed in the working fluid for 0, 24, 48, and

72 hours to study the effects of the non-boiling immersion time.

In each test run, the working fluid was first heated to the saturated temperature under atmospheric pressure, i.e. 56℃, for the saturated pool boiling experiment using the Fisher 90 Refrigerated Bath. For the 5 K subcooled boiling case, the working fluid was heated to 51℃. Then the cold water was opened to run through the condenser, which will change the FC-72 vapor back to liquid state. Once the test liquid reached its saturation temperature, it was left at this stage for 2 hours for degassing purposes. During this interval, insulation layers were applied outside the water bath vessel to prevent the heat losses.

After the degassing process, data acquisition was initiated. The heat-flux was controlled by varying the input voltages using the Variable Autotransformer. Starting from 20V, the voltage was first increased to 120V in a step by step process with an increment of 10V, and then decreased from 120V to 20V with a decrement of 10V. When the power to the cartridge heater was turned on, about 12 minutes were needed to reach steady state conditions. After that, a steady-state condition was usually reached 8 minutes after each voltage increase. This was verified by the experimental data (see Appendix A). The surface temperature and bulk fluid temperature were measured when steady-state was reached. After all the data were collected, the cartridge heater was powered off, but the water for the condenser was kept running until the FC-72 bulk temperature reached room temperature to prevent loss of the FC-72. Then the test section was removed and the FC-72 was carefully poured back into the storage container.

CHAPTER 3

RESULTS AND DISCUSSION

The data were analyzed and boiling curves of test surfaces under different conditions were plotted. In the plot, the x-axis was the wall surface superheat in K and the y-axis was the heat flux in W/m^2K. Heat flux was calculated using the power input of the cartridge heater divided by the upper surface area of the copper block.

3.1 POOL BOILING ENHANCEMENT OF POROUS COATED SURFACES

3.1.1 Saturated Pool Boiling

Figure 3.1 shows the saturated pool boiling curves of the three surfaces. In the natural convection section of the curves, the SSS has higher heat flux than the HFS at any given surface superheat. This may be due to the fact that there might have been some gases trapped in the micro-cavities of the HFS and this porous coated layer reduced the heat transfer in the natural convection region.

After the start of nucleate boiling, the SSS has the highest surface superheat and the lowest boiling heat transfer coefficient at a constant heat flux among the three surfaces, which can be seen in Figure 3.1. The EDS demonstrated lower heat flux values than those of the HFS for a specified surface superheat. This means that the HFS has a better nucleate boiling heat transfer performance than the EDS. The saturated boiling experimental data show that at the same heat flux value (6.6 k/m^2), the EDS experiences an enhancement in the boiling heat transfer coefficient by 75%, while the

Figure 3.1 Boiling curves of different surfaces in saturated FC-72 with 72 hours of non-boiling immersion time.

HFS by 276% compared to the SSS. From Figure 3.1, it can be seen that compared with the SSS (18.2 K), the boiling incipience superheat of the EDS (5.9 K) is reduced by 12.3 K (68%), while that of the HFS (8.5 K) reduced by 9.7 K (53%). This means that porous-coated surfaces can reduce the boiling incipience superheat.

For both the subcooled and saturated boiling conditions, the nucleate boiling of the SSS occurs at a much higher surface superheat than that of the HFS or the EDS. This is due to the fact that the SSS has lower site density than the porous coated surfaces, and thus requires a higher surface temperature to dissipate the same amount of heat as the porous coated surfaces.

According to Kim and Rainey [24], the increased heat transfer coefficients of the microporous surfaces are not because of the increased area generated by the microporous coating. This enhancement is a direct result of its significantly higher active nucleation site density. Rainey and You [34] showed that an increase in surface area shifts the boiling curve vertically, not horizontally, and has a significant effect only on the single phase natural convection heat transfer.

Many researchers believe that the nucleate boiling enhancement from porous-coated surfaces is the result of increased active nucleation site density. Kurihara and Myers [25] proposed that the increased numbers of nucleation sites may enhance the heat transfer by providing more convection heat transfer from increased bubble agitation and/or increased latent heat transfer.

The difference of boiling heat transfer enhancement between the EDS and the HFS can be interpreted as follows. As can be seen in Figure 2.5, the HFS is characterized with re-entrant cavities, which are absent on the EDS (see Figure 2.6).

Griffith and Wallis [18] demonstrated that the geometry of the microcavity containing trapped vapor was directly related to the bubble nucleation process. They found that the re-entrant type cavities were stable, easily activated boiling sites. In this work, since FC-72 is a highly-wetting fluid, the porous matrix of the EDS and the HFS was easily flooded with FC-72. But the re-entrant cavities in the HFS trapped more non-condensable gases than in the EDS which served as active nucleation sites during boiling incipience.

3.1.2 Subcooled Pool Boiling

When the bulk liquid temperature is less than the saturation temperature, subcooled boiling can occur on the heated surface if the surface temperature is sufficiently higher than the saturation temperature. Figure 3.2 shows the pool boiling curves of the three different surfaces with 5K subcooling of the working fluid. The SSS has the largest surface superheat for nucleate boiling (22.6K), which is larger than those of the EDS (6.9K) and HFS (9.5K). In other words, compared to the SSS, the EDS reduced the nucleate boiling superheat by 15.7 K (69%), while the HFS reduced it by 13.1 K (58%). This demonstrates that porous coated surfaces reduce the superheat of boiling incipience.

The 5 K subcooled boiling experimental data show that at the same heat flux value (6.6 k/m^2), the EDS increases the boiling heat transfer coefficient by 80%, while the HFS increases it by 239% compared to the SSS.

From Figure 3.3, 3.4, and 3.5 it can be found that the incipience superheats in
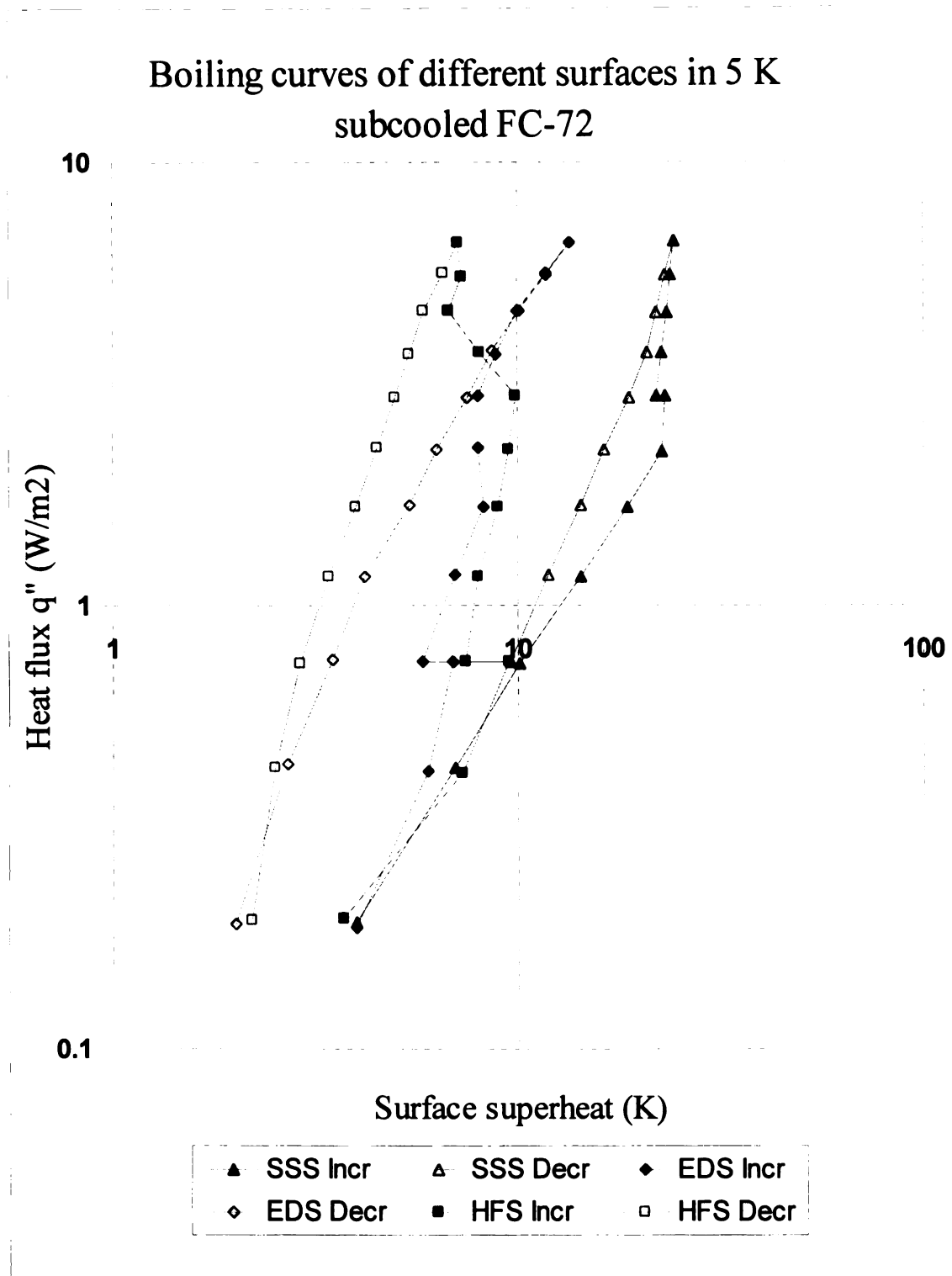
Figure 3.2 Boiling curves of different surfaces in 5 K subcooled FC-72 with 72 hours of non-boiling immersion time.

subcooled boiling were higher than those of the saturated cases. This was anticipated because in subcooled boiling as the bubbles departed from the heated surfaces, subcooled liquid filled the spaces left by the departing bubbles. It would take some time for the filling subcooled liquid to reach saturation conditions.

From Figure 3.3, 3.4, and 3.5 it can be seen that subcooling makes the boiling curves move to the right, whether the surfaces are super smooth surface or porous coated surfaces. Because the subcooled heat transfer coefficient is defined as [42]

$$\alpha_{sub} \equiv \frac{q}{T_w - T_b} \tag{3.1}$$

it decreases as the bulk liquid temperature T_b decreases.

Hui and Thome [20] studied the effect of liquid subcooling on the nucleate boiling curve of benzene boiling on a vertical brass disk. Their results demonstrate that even small levels of subcooling can substantially affect the heat transfer process and significantly reduce the boiling heat transfer coefficient.

From the boiling curves of the SSS (Figure 3.3) and the EDS (Figure 3.4) it is observed that the fully developed nucleate boiling curves of the subcooled cases collapsed on the curves of the saturated cases. This observation is consistent with the results of Rainey and You [34]. They tested the effect of subcooling on the pool boiling of microporous surfaces in FC-72 with a liquid subcooling range of 0 (saturation) to 50 K. Due to the restriction of the heater power, not enough data were collected to plot the fully developed boiling curves of the HFS for the subcooled case (Figure 3.5) in this study.
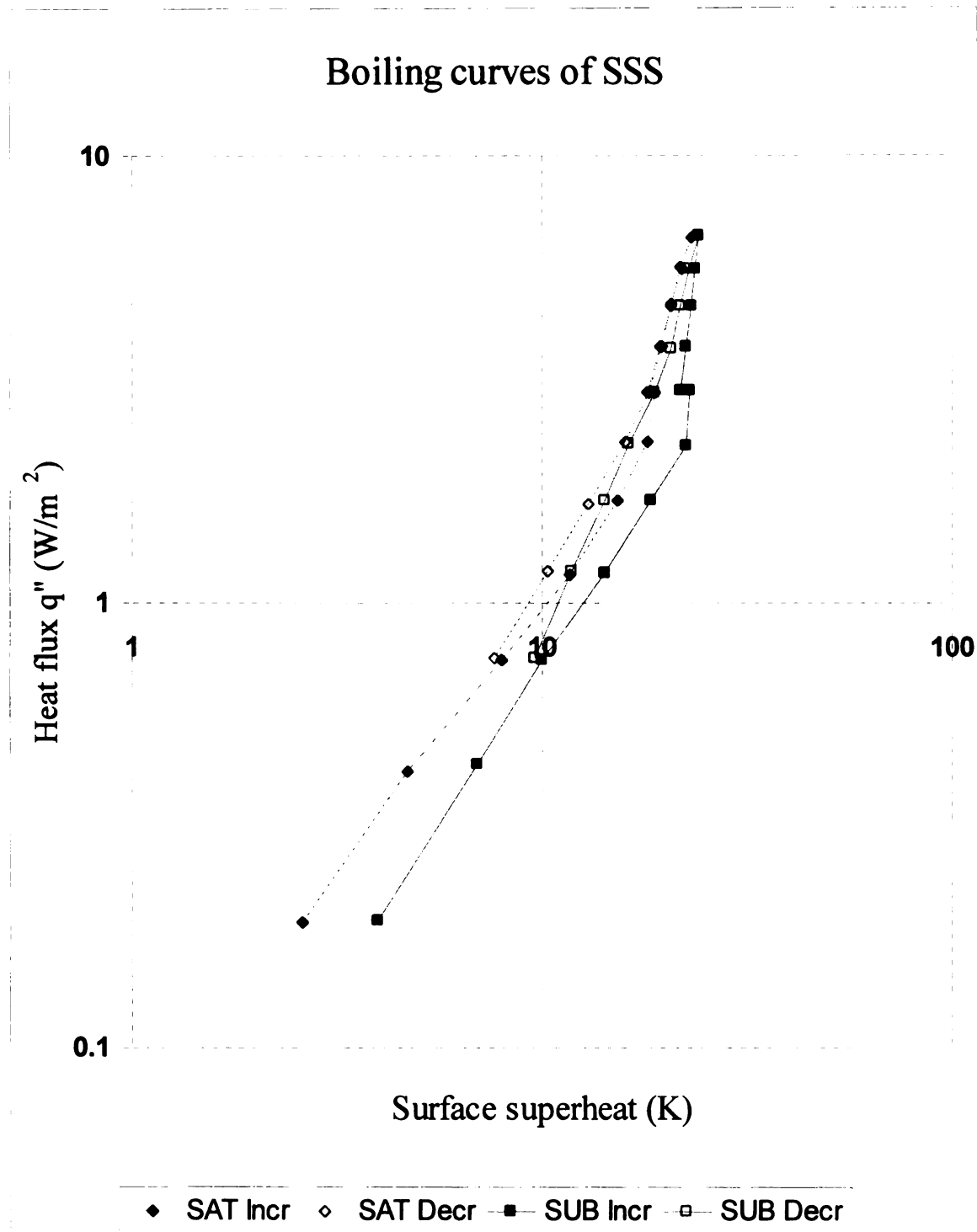
Figure 3.3 Boiling curves of SSS in 5K subcooled and saturated FC-72 with 72 hours of non-boiling immersion time.

Boiling curves of EDS
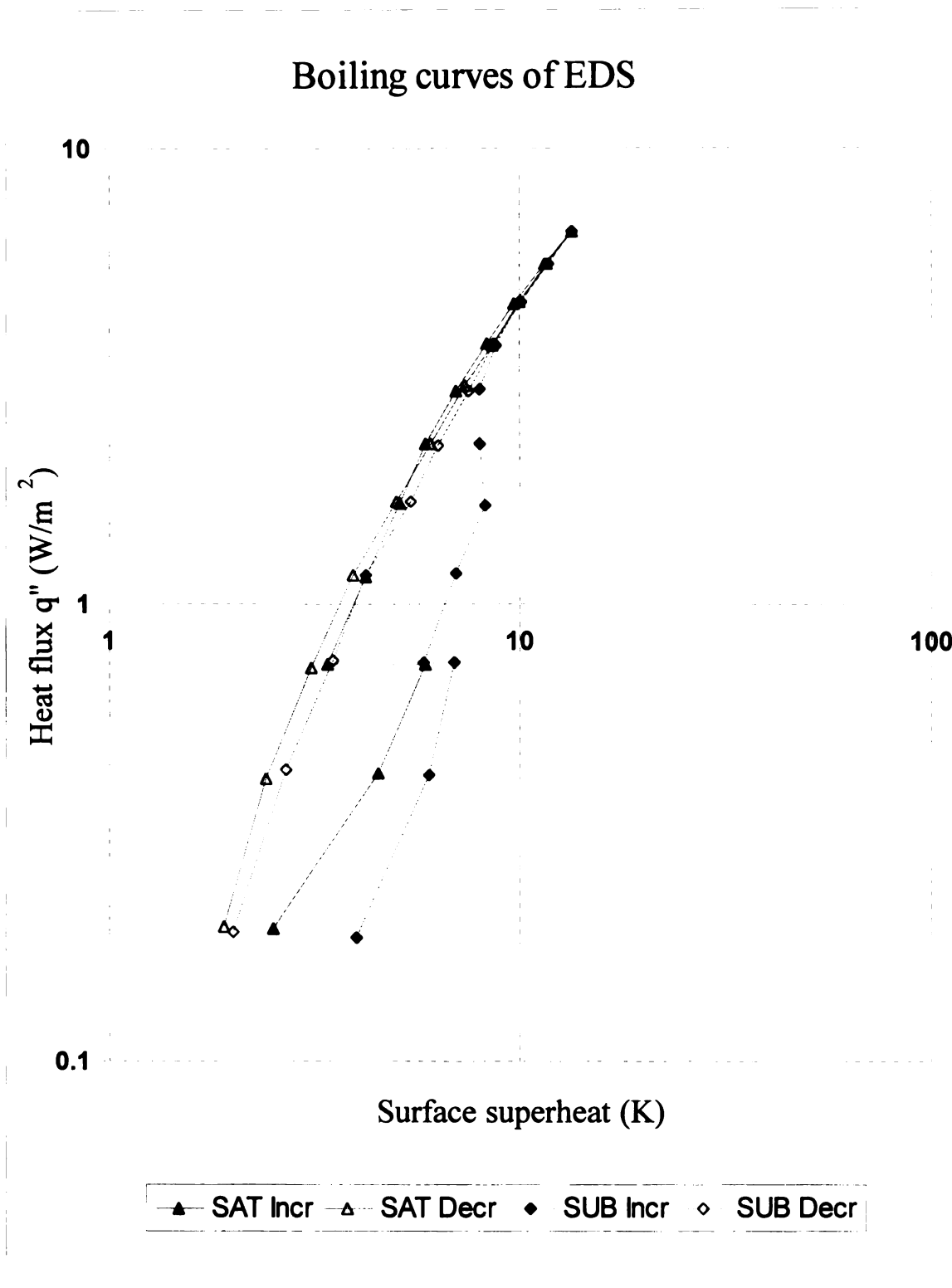
Figure 3.4 Boiling curves of EDS in 5K subcooled and saturated FC-72 with 72 hours of non-boiling immersion time.
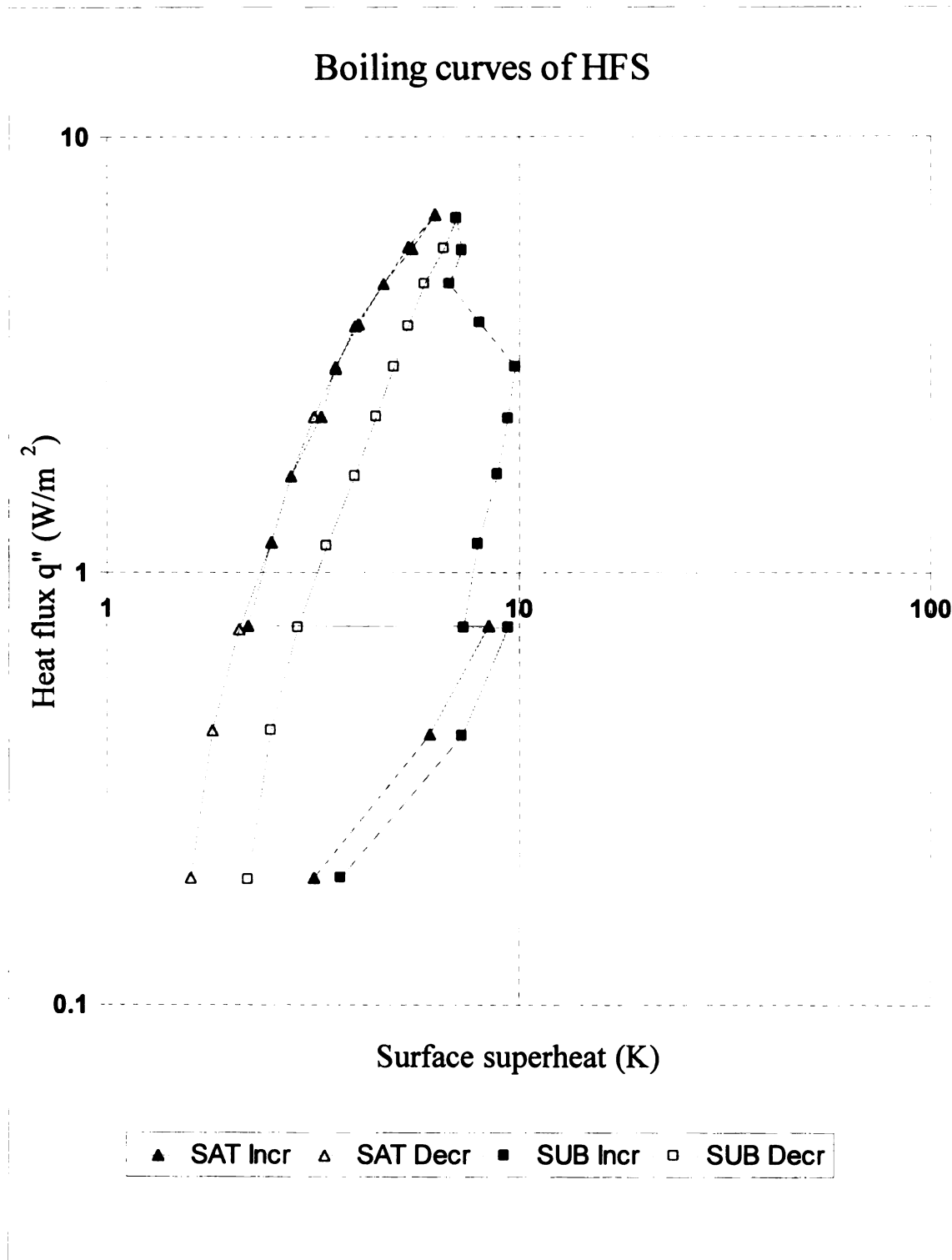
Figure 3.5 Boiling curves of HFS in 5K subcooled and saturated FC-72 with 72 hours of non-boiling immersion time.

The boiling curves in Figure 3.2 show that the subcooling does influence the natural convection part and the initial nucleate boiling part of the boiling curve. It was found that the subcooled pool boiling on porous coated surfaces is characterized by a phenomenon of patch boiling, which can be seen from the boiling curves of increased heat flux. Figure 3.6 shows the patch boiling of the HFS in 5 K subcooled FC-72. This phenomenon can be explained by flooding of the porous matrix with liquid so that only relatively small sites are available to act as active nucleation sites [8]. The distribution of the active nucleate sites on the surface was random. After vapors were generated from these active nucleate sites, they were quenched by the subcooled liquid in the vicinity before it can spread over the surface and activated other sites.

3.2 EFFECTS OF NONBOILING IMMERSION TIME

Figure 3.7 shows the boiling curves of HFS in 5K subcooled FC-72 with a non-boiling immersion time of 0 hour, 24 hours, 48 hours, and 72 hours. The experimental data of 0 hour and 24 hours showed that the non-boiling immersion can affect the temperature overshoot of incipient boiling, as is seen in Table 3.1.

As the non-boiling immersion time increasing, more and more microcavities in the porous matrix, which served as the active nucleate sites, were flooded with the low contact angle working liquid. When this happens, a very large wall superheat may be needed to activate the nucleate sites. After the starting of nucleate boiling, the heat transfer coefficient was dramatically increased due to the existence of phase change. So a smaller wall superheat was needed to transfer the same amount of heat.
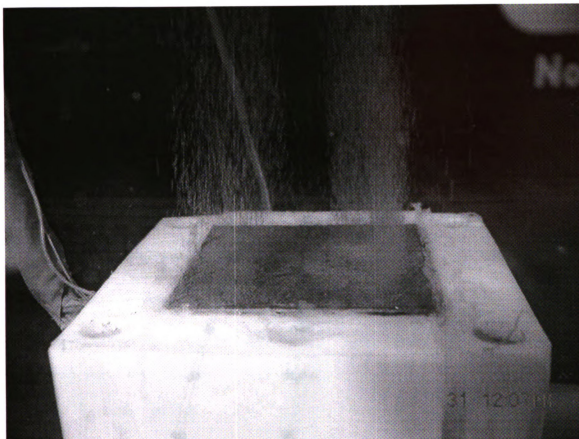
Figure 3.6 Patch boiling of HFS in 5 K subcooled FC-72 with 72 hours of non-boiling immersion time.

Table 3.1 Effect of non-boiling immersion time on incipient superheat and temperature overshoot.

Time of non-boiling immersion (Hours)	Surface superheat before incipient boiling (K)	Surface superheat after incipient boiling (K)	Temperature overshoot (K)
0	8.4	8.1	0.3
24	8.9	7.4	1.5
48	9.6	7.8	1.8
72	9.5	7.4	2.1
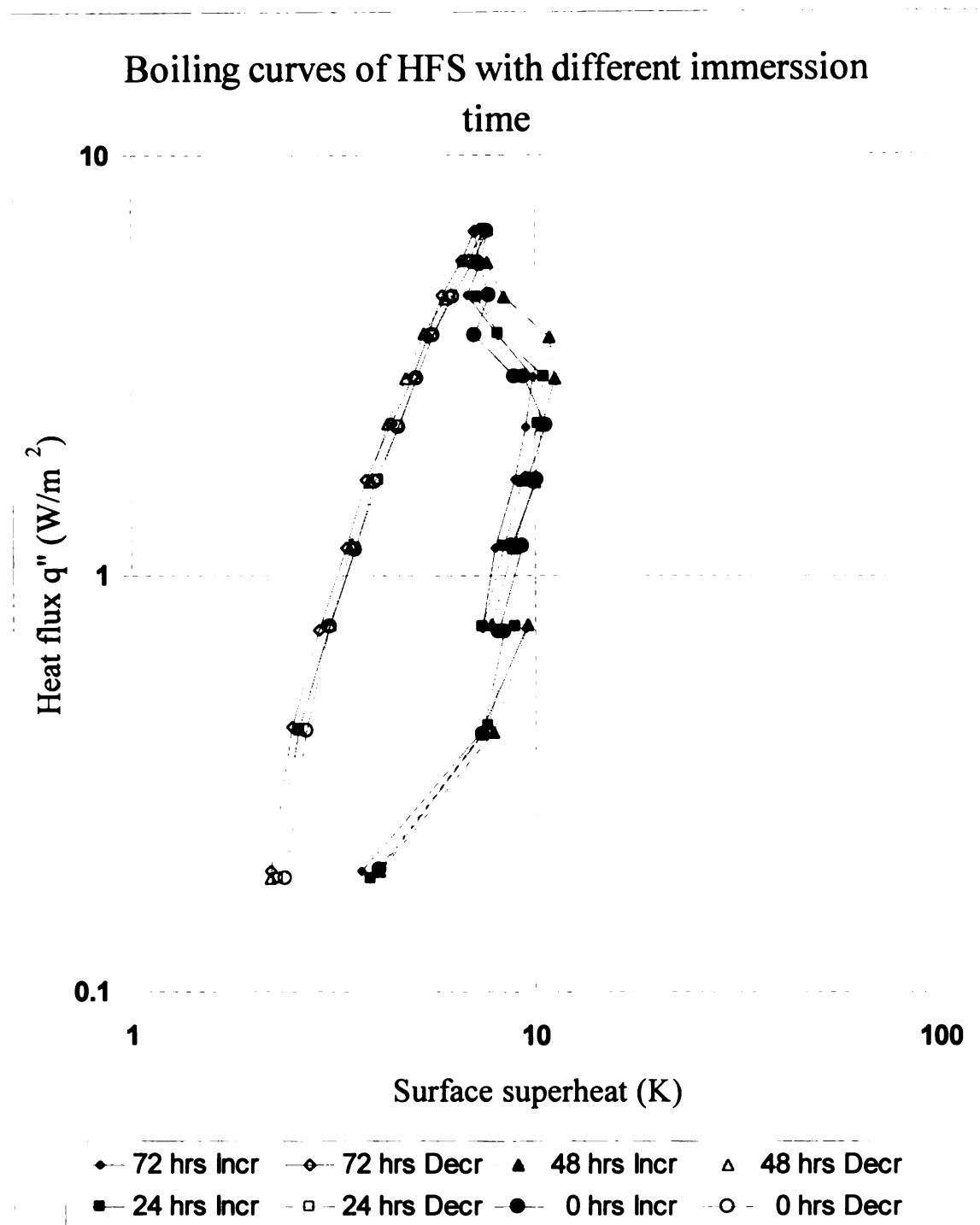
Figure 3.7 Boiling curves of HFS in 5K subcooled FC-72 with different non-boiling immersion time.

But after immersion times of 24 hours and greater, the temperature overshoot shows no dependence on the immersion time. This is in consistent with the conclusions of Miller et al [29]. They believe that once the noncondensable were removed from the cavities, the surface reached a steady condition in which the nucleation sites continue to retain vapor embryos.

3.3 BOILING HYSTERESIS PHENOMENON

The data presented in Figure 3.1 indicate that HFS is characterized by a large temperature overshoot which leads to dramatic boiling curve hysteresis. The free convection curve was followed typically until about $\Delta T=8.5K$ when there was an explosive formation of vapor, which reduce ΔT to 2.1K. The HFS temperature overshoot was 6.4 K, which was larger than that of the EDS (2.5 K). The SSS showed no temperature overshoot in the saturated pool boiling case.

Due to the irregularities of various hysteresis curves, the use of temperature difference is not enough to completely describe the hysteresis characteristics. Shi et al [38] introduced a parameter called hysteresis area, which is defined as the shaded area enclosed by the normal boiling curve and the hysteresis curve, as shown in Figure 3.8.

Comparing the hysteresis areas in Figure 3.3, 3.4, and 3.5, it is obvious that the HFS has the largest area, while the SSS has the smallest one. In other words, the boiling hysteresis phenomenon is the most prominent on the HFS among the three surfaces. For the same surface, the hysteresis area of subcooled boiling is larger than that in the saturated boiling case. So it can be concluded that subcooling can deteriorate the

boiling hysteresis phenomenon.
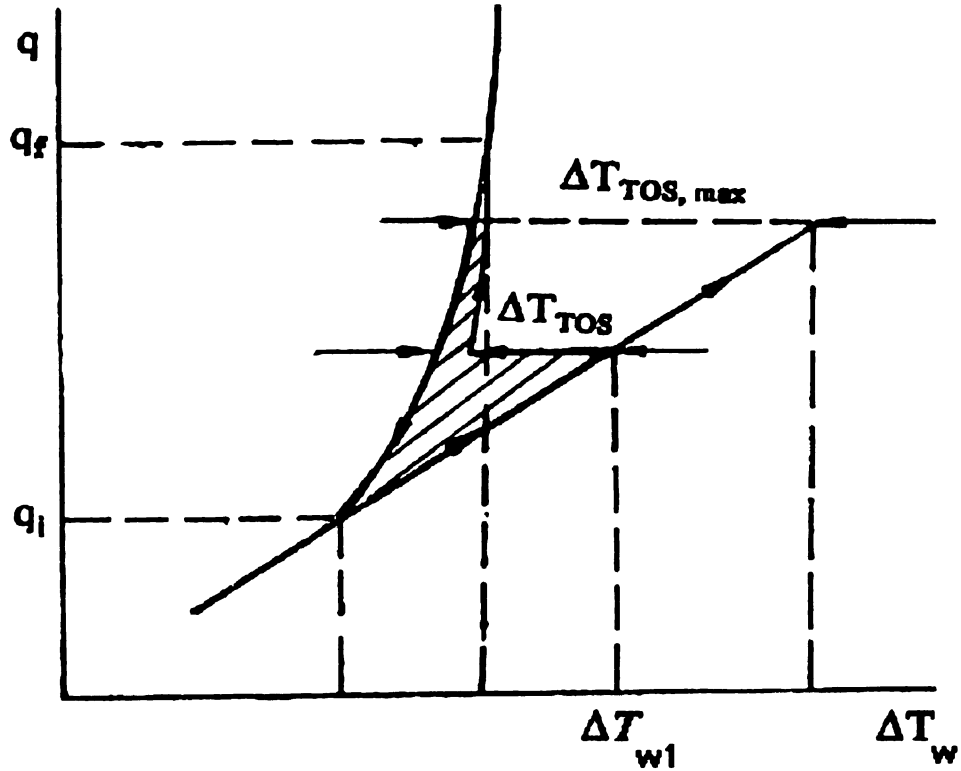
Figure 3.8 Hysteresis area [38].

3.4 BOILING CURVES WITH WATER AS WORKING FLUID

Ngai [33] and Aitcheson [1] studied the nucleate boiling heat transfer performance of these three surfaces with 10 K subcooled water as working fluid. They used a cartridge heater with much higher power than the one used in this study. Figure 3.9 shows the boiling curves plotted using their data. From this figure it can be seen
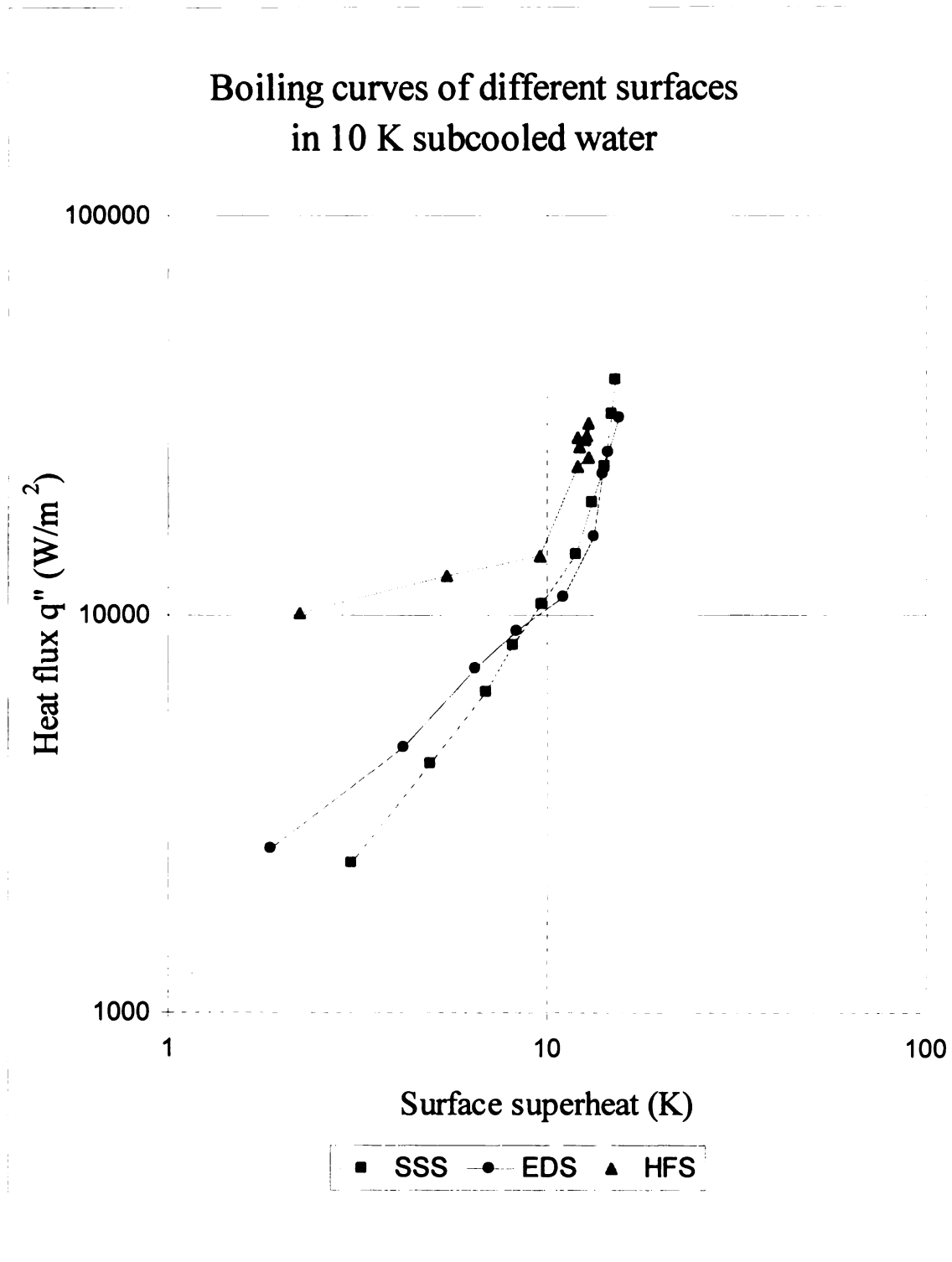
Figure 3.9 Boiling curves of different surfaces in 10 K subcooled water.

that in the natural convection region, for a given superheat, the SSS has the smallest convection heat transfer coefficient, the EDS has the medium one, while the HFS has the largest one.

In Figure 3.9, the EDS shows no prominent heat transfer enhancement compared to the SSS after incipience of boiling, whereas that of the HFS is obvious. There is no temperature overshoot in the EDS curve, but there some small ones in the HFS curve. This is probably due to different contact angles of water and FC-72. Since water has large contact angle and low-wetting ability than FC-72, the liquid penetration into the microcavities in the water test should be less than in the FC-72 test. The sizes of microcavities in the HFS are lager than those in the EDS, so more potential active nucleation sites in the HFS are flooded with water than in the EDS. This interprets the temperature overshoots in the HFS curve.

CHAPTER 4

SOCIAL AND ETHICAL CONSIDERATIONS

In this study, the fluid employed is FC-72, a highly-wetting dielectric perfluorocarbon (PFC) with zero ozone-depletion potential (ODP). So using FC-72 as working fluid will not destroy the ozone layer. This creates the potential for electronic cooling application. FC-72 is low-solubility substance and has insignificant toxicity to aquatic organisms. PFCs have high global warming potentials (GWP) so precautions should be taken to prevent direct release of this substance to the environment. If FC-72 is exposed to extreme conditions of heat from misuse or equipment failure, toxic decomposition products that include hydrogen fluoride and perfluoroisobutylene can occur [47].

The porous-coated surfaces can be widely applied in boilers, heat exchangers, heat pipes, and electronic cooling. Since these surfaces can dramatically enhance the boiling heat transfer performance, this can decrease the energy consumption and bring considerable social benefit.

CHAPTER 5

CONCLUSIONS

Three different surfaces, including the super-smooth surface (SSS), the High Flux ™ surface (HFS), and the electrochemical deposition surface (EDS) were tested in the experimental study of pool boiling behavior in subcooled and saturated FC-72. The effects of subcooling and non-boiling immersion time were investigated. Following are the primary conclusions from this study:

1. Microporous coatings enhance nucleate boiling heat transfer due to their significantly higher nucleation site density. Compared with the smooth surface, the porous-coated surface can reduce the superheat of boiling incipience and increase the boiling heat transfer coefficient.

2. Subcooling does not appear to influence the fully developed part of the boiling curve comparing with the saturated boiling curve, but it does influence the natural convection part and the initial nucleate boiling part of the boiling curve. The subcooled pool boiling on porous coated surfaces is characterized by a phenomenon of patch boiling. The subcooling makes the boiling curves move to the right.

3. The boiling hysteresis phenomenon is more prominent on porous-coated surface than on the smooth surface, but subcooling is shown to deteriorate the boiling hysteresis.

4. Non-boiling immersion was seen to increase the temperature overshoot of incipient boiling. But after immersion times of 24 hours and greater, the temperature

overshoot shows no dependence on the immersion time.

5. The HFS enhanced the nucleate boiling heat transfer performance more effectively than the EDS, but the EDS has smaller boiling incipient superheat and Temperature Overshoot and Temperature Deviation hysteresis, which provides the EDS potential for industrial application.

6. The contact angle of the working fluid was a significant influence on the boiling hysteresis and the temperature overshoots.

CHAPTER 6

RECOMMENDATIONS

Suggestions for future work in the area of nucleate pool boiling from porous-coated surfaces in FC-72 are as follows:

1. Rebuild the test section with a larger power cartridge heater and investigate the CHF of porous-coated surfaces and compare it with that of the smooth surface.

2. Study the bubble dynamics of the nucleate pool boiling from porous-coated surfaces with FC-72 as the working fluid, including the bubble departure diameter, frequency etc to investigate the boiling enhancement mechanism more thoroughly.

3. Investigate the possible solutions to diminish boiling hysteresis phenomenon on porous-coated surfaces in order to secure these surfaces to work more effectively in the industrial application.

APPENDICES

APPENDIX A

STEADY STATE VERIFICATION

When increasing the heat flux by increasing the voltage input of the heater, a steady state is needed before the acquisition of data. An experiment was conducted to find the time interval necessary to reach the steady state.

The power of the cartridge heater was increased by increments of 10 Volts. Temperature data of the surface were taken very minute. The data showed in the table below and in Figure A.1 verified that when the power of cartridge heater was turned on, about 12 minutes were needed to reach the steady state condition. After that, a steady-state condition was usually reached 8 minutes after each voltage increase.

Table A.1 Change of surface temperature after each voltage increase

Voltage (V)	Time (min)	Temp. for TC #1 (°C)
20.4	1	50.7
	2	51.5
	3	51.9
	4	52.3
	5	52.7
	6	53
	7	53.2
	8	53.5
	9	53.5
	10	53.6
	11	53.7
	12	53.7
	13	53.8
	14	53.8
	15	53.8
25.4	16	54.1
	17	54.4
	18	54.7

	19	54.8
	20	55
	21	55.2
	22	55.1
	23	55.2
	24	55.2
	25	55.1
30.5	26	55.6
	27	56
	28	56.3
	29	56.5
	30	56.6
	31	56.7
	32	56.8
	33	56.9
	34	56.8
	35	56.9
	36	57
	37	57
40.5	38	58
	39	58.8
	40	59.4
	41	59.6
	42	59.8
	43	60
	44	60
	45	60
	46	60.1
	47	60.2
	48	60.1
	49	60.2
	50	60.1
	51	60.1
50.5	52	61.2
	53	60
	54	59.3
	55	59.2
	56	59.2
	57	59.1
	58	59.1
	59	59.2
	60	59.1
	61	59.1
	62	59.2
60.7	63	60
	64	60.2

	65	60.3
	66	60.5
	67	60.4
	68	60.5
	69	60.5
	70	60.5
	71	60.6

Surface temperature vs. heating time

◆ 20.4V ■ 25.4V ▲ 30.5V × 40.5V × 50.5V ● 60.7V
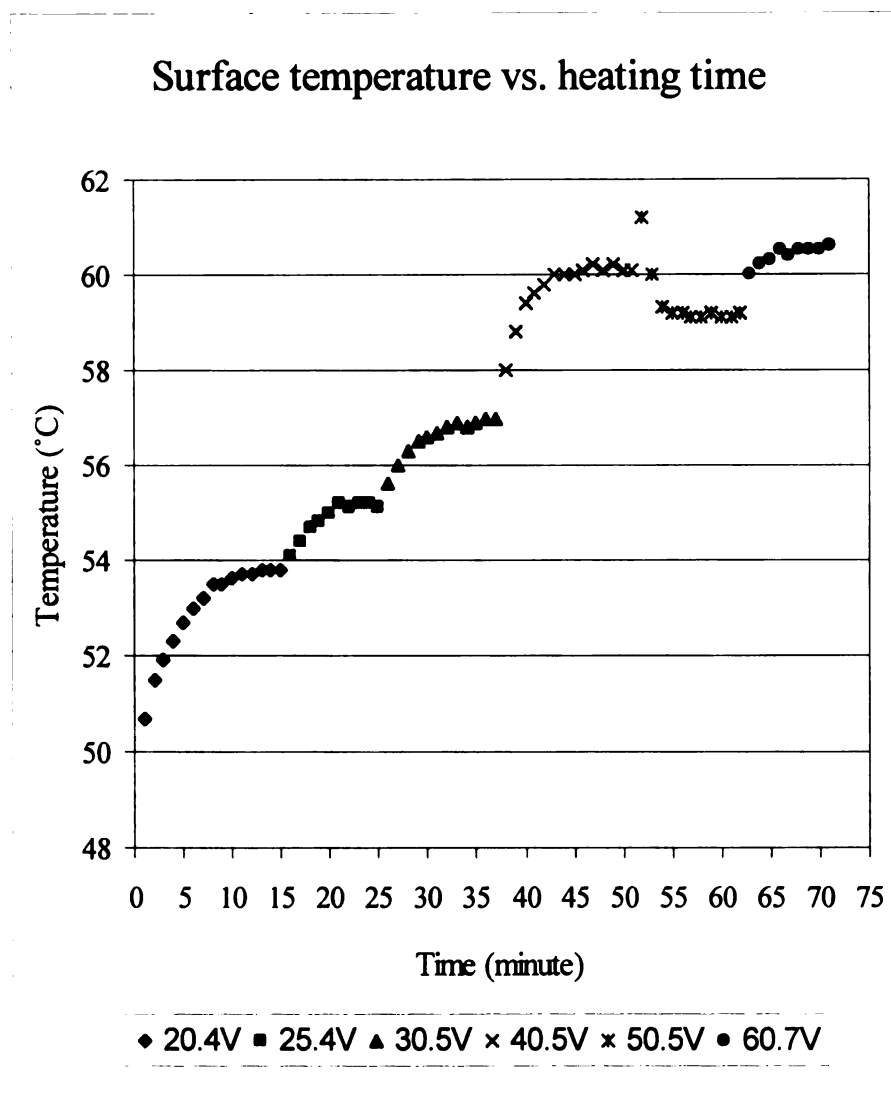
Figure A.1 Change of surface temperature after each voltage increase.

APPENDIX B

EXPERIMENTAL DATA

Table B.1 Experimental data of the SSS in 5K subcooled FC-72
with 72 hours of non-boiling immersion time.

Increased heat flux						
Voltage (V)	Heat Flux (W/m^2)	TC#1 (°C)	TC#2 (°C)	T Avg (°C)	T Bulk (°C)	Superheat (K)
20.6	0.192459799	55.6	55.7	55.7	51.7	4
30.8	0.430236271	58.4	58.4	58.4	51.4	7
40.4	0.740232788	61.2	61.3	61.3	51.2	10.1
50.6	1.161198914	65.4	65.4	65.4	51.1	14.3
60.7	1.671025086	69.5	69.6	69.6	51	18.6
70.1	2.228648736	73.8	73.8	73.8	51.2	22.6
80.8	2.960931151	76.4	76.4	76.4	53.3	23.1
80.8	2.960931151	75.2	75.3	75.3	53.3	22
90.5	3.714520383	77.2	77.2	77.2	54.5	22.7
100.5	4.580761821	78.6	78.7	78.7	55.4	23.3
110.6	5.547736706	79.8	79.8	79.8	56	23.8
120.7	6.60724069	80.8	80.9	80.9	56.6	24.3
Decreased heat flux						
Voltage (V)	Heat Flux (W/m^2)	TC#1 (°C)	TC#2 (°C)	T Avg (°C)	T Bulk (°C)	Superheat (K)
120.7	6.60724069	80.8	80.9	80.9	56.6	24.3
110.7	5.557773315	79.5	79.5	79.5	56.4	23.1
100.5	4.580761821	78.3	78.3	78.3	56.3	22
90.4	3.706316034	76.9	77	77	56.2	20.8
80.5	2.938984856	74.9	74.9	74.9	56	18.9
70.3	2.241383846	72.2	72.2	72.2	55.8	16.4
60.9	1.682054924	69.1	69.1	69.1	54.8	14.3
50.8	1.170396494	64.7	64.8	64.8	52.9	11.9
40.6	0.747579966	60.6	60.6	60.6	51	9.6
30.4	0.419133867	57.7	57.6	57.6	49.8	7.8
20.8	0.196215024	54.2	54.2	54.2	48.6	5.6

Table B.2 Experimental data of the SSS in saturated FC-72 with 72 hours of non-boiling immersion time.

Increased heat flux						
Voltage (V)	Heat Flux (W/m^2)	TC#1 (°C)	TC#2 (°C)	T Avg (°C)	T Bulk (°C)	Superheat (K)
20.5	0.190595793	59.4	59.5	59.5	56.9	2.6
30.3	0.416380943	61.3	61.3	61.3	56.6	4.7
40.5	0.743901842	64.2	64.2	64.2	56.2	8
50.4	1.152037618	67.8	67.9	67.9	56.1	11.8
60.7	1.671025086	71.5	71.5	71.5	56.1	15.4
70.9	2.279806869	74.6	74.7	74.7	56.5	18.2
80.3	2.924399345	75.9	75.9	75.9	57	18.9
80.3	2.924399345	75.2	75.2	75.2	57	18.2
90.5	3.714520383	76.4	76.5	76.5	57	19.5
100.6	4.5898823	78	78	78	57.2	20.8
110.9	5.577873745	79.2	79.3	79.3	57.3	22
120.2	6.552613056	80.7	80.7	80.7	57.3	23.4
Decreased heat flux						
Voltage (V)	Heat Flux (W/m^2)	TC#1 (°C)	TC#2 (°C)	T Avg (°C)	T Bulk (°C)	Superheat (K)
120.2	6.552613056	80.7	80.7	80.7	57.3	23.4
110.8	5.567818995	79.4	79.4	79.4	57.3	22.1
101	4.626454923	78.1	78.1	78.1	57.3	20.8
90.8	3.739187856	76.8	76.9	76.9	57.2	19.7
80.6	2.946291217	75.4	75.4	75.4	57.1	18.3
70.8	2.273380355	73.1	73.1	73.1	57	16.1
60.3	1.649074255	70	70	70	56.9	13.1
50.8	1.170396494	66.5	66.6	66.6	56.2	10.4
30.5	0.421895862	59.5	59.5	59.5	50.1	9.4
40.6	0.747579966	62.5	62.6	62.6	54.9	7.7
20.5	0.190595793	56.7	56.7	56.7	49.2	7.5

Table B.3 Experimental data of the EDS in 5K subcooled FC-72
with 72 hours of non-boiling immersion time.

Increased heat flux						
Voltage (V)	Heat Flux (W/m²)	TC#1 (°C)	TC#2 (°C)	T Avg (°C)	T Bulk (°C)	Superheat (K)
20.3	0.186894992	56.8	56.8	56.8	52.8	4
30.5	0.421895862	58.5	58.5	58.5	52.5	6
40.6	0.747579966	59.1	59.2	59.2	52.3	6.9
40.6	0.747579966	58.1	58.1	58.1	52.3	5.8
50.8	1.170396494	59.2	59.2	59.2	52.2	7
60.5	1.660031529	60.3	60.3	60.3	52.1	8.2
70.5	2.254155238	61.2	61.3	61.3	53.3	8
81	2.975607367	62.7	62.7	62.7	54.7	8
90.1	3.681757409	64.2	64.2	64.2	55.4	8.8
100.9	4.617298161	65.9	66	66	56	10
111	5.587937565	68	68	68	56.2	11.8
120.3	6.563520441	69.8	69.8	69.8	56.4	13.4
Decreased heat flux						
Voltage (V)	Heat Flux (W/m²)	TC#1 (°C)	TC#2 (°C)	T Avg (°C)	T Bulk (°C)	Superheat (K)
120.3	6.563520441	69.8	69.8	69.8	56.4	13.4
110.8	5.567818995	68	68	68	56.2	11.8
100.8	4.60815047	66.1	66.1	66.1	56	10.1
90.8	3.739187856	64.2	64.3	64.3	55.6	8.7
80.4	2.931687565	62.6	62.6	62.6	55.1	7.5
70.2	2.235011755	61.1	61.1	61.1	54.8	6.3
60.8	1.67653547	60.1	60.1	60.1	54.7	5.4
50.5	1.156613731	58.6	58.7	58.7	54.5	4.2
40.8	0.754963427	57.8	57.8	57.8	54.3	3.5
31	0.435841896	56.8	56.8	56.8	54.1	2.7
20.5	0.190595793	55.1	55.1	55.1	53.1	2

Table B.4 Experimental data of the EDS in saturated FC-72
with 72 hours of non-boiling immersion time.

Increased heat flux						
Voltage (V)	Heat Flux (W/m²)	TC#1 (°C)	TC#2 (°C)	T Avg (°C)	T Bulk (°C)	Superheat (K)
20.7	0.194332876	58.1	58.1	58.1	55.6	2.5
30.7	0.427447064	59.8	59.8	59.8	55.3	4.5
40.4	0.740232788	61.1	61.2	61.2	55.3	5.9
40.4	0.740232788	58.7	58.7	58.7	55.3	3.4
50.4	1.152037618	59.4	59.4	59.4	55.2	4.2
60.7	1.671025086	60.3	60.4	60.4	55.3	5.1
70.6	2.26055454	61.5	61.5	61.5	55.6	5.9
80.4	2.931687565	62.8	62.8	62.8	55.8	7
90.5	3.714520383	64.4	64.5	64.5	56.2	8.3
100.4	4.571650412	66.2	66.2	66.2	56.5	9.7
110.7	5.557773315	68	68	68	56.5	11.5
120.3	6.563520441	69.9	70	70	56.6	13.4
Decreased heat flux						
Voltage (V)	Heat Flux (W/m²)	TC#1 (°C)	TC#2 (°C)	T Avg (°C)	T Bulk (°C)	Superheat (K)
120.3	6.563520441	69.9	70	70	56.6	13.4
110.7	5.557773315	68.1	68.1	68.1	56.5	11.6
100.6	4.5898823	66.2	66.2	66.2	56.2	10
90.1	3.681757409	64.4	64.5	64.5	55.9	8.6
81.5	3.012456643	63	63	63	55.6	7.4
70.5	2.254155238	61.5	61.5	61.5	55.4	6.1
60.9	1.682054924	60.2	60.2	60.2	55.2	5
50.6	1.161198914	58.9	59	59	55.1	3.9
40	0.725647277	58	58	58	54.9	3.1
30.3	0.416380943	56.9	57	57	54.6	2.4
20.8	0.196215024	56.3	56.3	56.3	54.4	1.9

Table B.5 Experimental data of the HFS in 5K subcooled FC-72
with 72 hours of non-boiling immersion time.

Increased heat flux						
Voltage (V)	Heat Flux (W/m²)	TC#1 (°C)	TC#2 (°C)	T Avg (°C)	T Bulk (°C)	Superheat (K)
20.8	0.196215024	54.7	54.7	54.7	51	3.7
30.3	0.416380943	57.9	58	58	50.7	7.3
40.5	0.743901842	60.1	60.1	60.1	50.6	9.5
40.5	0.743901842	58	58	58	50.6	7.4
50.6	1.161198914	58.5	58.5	58.5	50.5	8
60.7	1.671025086	59.4	59.4	59.4	50.5	8.9
70.3	2.241383846	59.9	60	60	50.5	9.5
80.8	2.960931151	60.8	60.8	60.8	50.9	9.9
90.6	3.722733804	61.6	61.6	61.6	53.5	8.1
100.9	4.617298161	62.3	62.3	62.3	55.5	6.8
110.1	5.49768972	62.9	63	63	55.7	7.3
120.2	6.552613056	63.9	63.9	63.9	56.8	7.1
Decreased heat flux						
Voltage (V)	Heat Flux (W/m²)	TC#1 (°C)	TC#2 (°C)	T Avg (°C)	T Bulk (°C)	Superheat (K)
120.2	6.552613056	63.9	63.9	63.9	56.8	7.1
110.9	5.577873745	63.2	63.2	63.2	56.6	6.6
100.9	4.617298161	62.3	62.3	62.3	56.4	5.9
90.1	3.681757409	61.5	61.6	61.6	56.2	5.4
80.6	2.946291217	60.8	60.8	60.8	55.8	5
70.8	2.273380355	60.1	60.1	60.1	55.6	4.5
60.6	1.665523772	59.4	59.5	59.5	55.5	4
50.4	1.152037618	58.6	58.6	58.6	55.2	3.4
40.4	0.740232788	58	58	58	55.1	2.9
30.8	0.430236271	57.1	57.1	57.1	54.6	2.5
20.7	0.194332876	54.6	54.6	54.6	52.4	2.2

Table B.6 Experimental data of the HFS in saturated FC-72
with 72 hours of non-boiling immersion time.

Increased heat flux						
Voltage (V)	Heat Flux (W/m^2)	TC#1 (°C)	TC#2 (°C)	T Avg (°C)	T Bulk (°C)	Superheat (K)
20.8	0.196215024	59.9	59.9	59.9	56.7	3.2
30.4	0.419133867	62.4	62.4	62.4	56.3	6.1
40.7	0.751267162	64.6	64.7	64.7	56.2	8.5
40.7	0.751267162	58.4	58.4	58.4	56.2	2.2
50.7	1.165793169	58.7	58.7	58.7	56.2	2.5
60.6	1.665523772	59.1	59.1	59.1	56.3	2.8
70.6	2.26055454	59.6	59.7	59.7	56.4	3.3
80.6	2.946291217	60.2	60.2	60.2	56.6	3.6
90.5	3.714520383	60.8	60.8	60.8	56.7	4.1
100.8	4.60815047	61.4	61.5	61.5	56.8	4.7
111.4	5.628283554	62.2	62.2	62.2	56.8	5.4
121	6.640126117	63.1	63.1	63.1	56.8	6.3
Decreased heat flux						
Voltage (V)	Heat Flux (W/m^2)	TC#1 (°C)	TC#2 (°C)	T Avg (°C)	T Bulk (°C)	Superheat (K)
121	6.640126117	63.1	63.1	63.1	56.8	6.3
110.9	5.577873745	62.3	62.3	62.3	56.8	5.5
100.7	4.59901185	61.5	61.5	61.5	56.8	4.7
90	3.673589342	60.7	60.7	60.7	56.7	4
80.4	2.931687565	60.1	60.1	60.1	56.5	3.6
70.6	2.26055454	59.4	59.5	59.5	56.3	3.2
60.4	1.654548357	58.9	58.9	58.9	56.1	2.8
50.7	1.165793169	58.1	58.1	58.1	55.6	2.5
40.2	0.732921891	57.2	57.3	57.3	55.2	2.1
30.8	0.430236271	56.6	56.6	56.6	54.8	1.8
20.8	0.196215024	54.4	54.5	54.5	52.9	1.6

Table B.7 Experimental data of the HFS in 5K subcooled FC-72
with 48 hours of non-boiling immersion time.

Increased heat flux						
Voltage (V)	Heat Flux (W/m²)	TC#1 (°C)	TC#2 (°C)	T Avg (°C)	T Bulk (°C)	Superheat (K)
20.7	0.194332876	54.8	54.8	54.8	50.7	4.1
30.4	0.419133867	58.2	58.3	58.3	50.4	7.9
40.9	0.758668764	59.8	59.8	59.8	50.2	9.6
40.9	0.758668764	58	58	58	50.2	7.8
50.4	1.152037618	58.6	58.7	58.7	49.9	8.8
60.5	1.660031529	59.7	59.7	59.7	49.7	10
70.5	2.254155238	59.9	59.9	59.9	49.5	10.4
80.2	2.917120196	60.5	60.6	60.6	49.4	11.2
90.3	3.698120755	61.3	61.3	61.3	50.4	10.9
100.6	4.5898823	61.9	62	62	53.6	8.4
110.5	5.537709168	62.6	62.6	62.6	55	7.6
120.8	6.618193429	63.6	63.6	63.6	56	7.6
Decreased heat flux						
Voltage (V)	Heat Flux (W/m²)	TC#1 (°C)	TC#2 (°C)	T Avg (°C)	T Bulk (°C)	Superheat (K)
120.8	6.618193429	63.6	63.6	63.6	56	7.6
110.9	5.577873745	62.6	62.6	62.6	55.9	6.7
100.2	4.553454807	61.8	61.9	61.9	55.9	6
90.8	3.739187856	61.1	61.1	61.1	55.8	5.3
80.3	2.924399345	60.3	60.3	60.3	55.5	4.8
70.9	2.279806869	59.5	59.6	59.6	55.3	4.3
60.5	1.660031529	58.7	58.7	58.7	54.8	3.9
50.9	1.175008889	58.1	58.1	58.1	54.6	3.5
40.9	0.758668764	57.3	57.3	57.3	54.2	3.1
30.6	0.424666928	56.2	56.3	56.3	53.7	2.6
20.3	0.186894992	53.5	53.5	53.5	51.3	2.2

Table B.8 Experimental data of the HFS in 5K subcooled FC-72
with 24 hours of non-boiling immersion time.

Increased heat flux						
Voltage (V)	Heat Flux (W/m^2)	TC#1 (°C)	TC#2 (°C)	T Avg (°C)	T Bulk (°C)	Superheat (K)
20.3	0.186894992	54.9	54.9	54.9	51	3.9
30.9	0.433034548	58.2	58.2	58.2	50.6	7.6
40.7	0.751267162	59.5	59.5	59.5	50.6	8.9
40.7	0.751267162	57.9	58	58	50.6	7.4
50.8	1.170396494	58.8	58.8	58.8	50.4	8.4
60.5	1.660031529	59.6	59.6	59.6	50.3	9.3
70.8	2.273380355	60.5	60.5	60.5	50.3	10.2
80.8	2.960931151	61.3	61.4	61.4	50.9	10.5
91	3.75567819	61.1	61.1	61.1	53	8.1
100.7	4.59901185	61.8	61.8	61.8	54.6	7.2
110.9	5.577873745	62.5	62.6	62.6	55.4	7.2
120.8	6.618193429	63.5	63.5	63.5	56	7.5
Decreased heat flux						
Voltage (V)	Heat Flux (W/m^2)	TC#1 (°C)	TC#2 (°C)	T Avg (°C)	T Bulk (°C)	Superheat (K)
120.8	6.618193429	63.5	63.5	63.5	56	7.5
110.9	5.577873745	62.7	62.7	62.7	55.8	6.9
100.8	4.60815047	61.8	61.8	61.8	55.6	6.2
90.6	3.722733804	60.9	61	61	55.4	5.6
80.3	2.924399345	60.3	60.3	60.3	55.2	5.1
70.4	2.247765006	59.6	59.6	59.6	55	4.6
60.6	1.665523772	58.8	58.9	58.9	54.8	4.1
50.6	1.161198914	58.1	58.1	58.1	54.5	3.6
40.8	0.754963427	57.3	57.3	57.3	54.2	3.1
30.6	0.424666928	56.2	56.3	56.3	53.7	2.6
20.3	0.186894992	53.5	53.5	53.5	51.2	2.3

Table B.9 Experimental data of the HFS in 5K subcooled FC-72
with 0 hour of non-boiling immersion time.

Increased heat flux						
Voltage (V)	Heat Flux (W/m²)	TC#1 (°C)	TC#2 (°C)	T Avg (°C)	T Bulk (°C)	Superheat (K)
20.9	0.198106242	55.2	55.2	55.2	51.1	4.1
30.2	0.413637089	58.1	58.1	58.1	50.7	7.4
40.2	0.732921891	58.9	58.9	58.9	50.5	8.4
40.2	0.732921891	58.5	58.6	58.6	50.5	8.1
50.7	1.165793169	59.6	59.6	59.6	50.3	9.3
50.7	1.165793169	56.9	59	59	50.3	8.7
60.7	1.671025086	60.1	60.1	60.1	50	10.1
60.7	1.671025086	59.6	59.6	59.6	50	9.6
70.6	2.26055454	60.4	60.5	60.5	49.9	10.6
80.7	2.953606648	60.6	60.6	60.6	51.2	9.4
80.7	2.953606648	60.1	60.1	60.1	51.2	8.9
90.6	3.722733804	60.7	60.8	60.8	53.7	7.1
100.9	4.617298161	61.7	61.7	61.7	54	7.7
110.3	5.517681303	62.4	62.4	62.4	55.1	7.3
120.4	6.574436898	63.1	63.2	63.2	55.6	7.6
Decreased heat flux						
Voltage (V)	Heat Flux (W/m²)	TC#1 (°C)	TC#2 (°C)	T Avg (°C)	T Bulk (°C)	Superheat (K)
120.4	6.574436898	63.1	63.2	63.2	55.6	7.6
110.4	5.5276907	62.6	62.6	62.6	55.6	7
100.7	4.59901185	61.7	61.7	61.7	55.4	6.3
90.7	3.730956294	60.8	60.8	60.8	55.2	5.6
80.5	2.938984856	60.1	60.1	60.1	55	5.1
70.2	2.235011755	59.3	59.4	59.4	54.8	4.6
60.3	1.649074255	58.7	58.7	58.7	54.7	4
50.2	1.142912603	58	58	58	54.4	3.6
40.7	0.751267162	57.2	57.2	57.2	54.1	3.1
30.5	0.421895862	56.3	56.3	56.3	53.6	2.7
20.3	0.186894992	53.7	53.8	53.8	51.4	2.4

APPENDIX C

UNCERTAINTY ANALYSIS

C.1 Temperature Measurement Uncertainty

The last digit of reading from the OMEGA HH23 Microprocessor Thermometer was 0.1 °C, thus the uncertainty in the temperature measurement was 0.05 °C.

The uncertainties in measurements of the length and width of the upper surface, a and b, are

$$da = db = \pm 0.5mm = \pm 5 \times 10^{-4} m \qquad (C.1)$$

The uncertainties in measurements of the voltage input U and the resistance of the cartridge heater R are

$$dU = \pm 0.05V \qquad (C.2)$$

$$dR = \pm 0.05\Omega \qquad (C.3)$$

C.2 Heat Flux Uncertainty

Heat flux was calculated using the power input of the cartridge heater divided by the upper surface area of the copper block.

$$q'' = \frac{E}{A} \qquad (C.4)$$

where A is the area of the copper block upper surface.

The electric power generated by the cartridge heater

$$E = \frac{U^2}{R} \qquad (C.5)$$

The uncertainty of E becomes

$$dE = \left| \frac{\partial E}{\partial U} \right| dU + \left| \frac{\partial E}{\partial R} \right| dR$$

$$= \frac{2U}{R} dU + \frac{U^2}{R^2} dR \qquad \qquad (C.6)$$

$$= E \left(\frac{2dU}{U} + \frac{dR}{R} \right)$$

So it gives

$$\frac{dE}{E} = \frac{2dU}{U} + \frac{dR}{R} \qquad \qquad (C.7)$$

Similarly, the uncertainty of A is

$$\frac{dA}{A} = \frac{da}{a} + \frac{db}{b} \qquad \qquad (C.8)$$

In the calculation of the heat flux, it was assumed that all heat generated by the cartridge heater transferred through the upper surface of the copper block, where the test surface was soldered. Although Teflon has a good insulation effect, there was heat loss from the sides and bottom of the test section. This is a kind of systematic error.

Assume the inside temperature of Teflon sleeves T_{in} equals to the copper block temperature T_{in} and the outside temperature of Teflon sleeves T_{out} equals to the temperature of bulk liquid T_{bulk}. The heat losses by conduction through Teflon sleeves are

$$q_{loss}'' = -k \frac{T_{out} - T_{in}}{L} \qquad \qquad (C.9)$$

where k is the thermal conductivity of Teflon in W/m K and L is the thickness of Teflon sleeves in m. Since k is a function of temperature, here it is approximated with the value under the average temperature of T_{in} and T_{out}. Then the systematic error is

71

$\dfrac{q_{loss}^{''} A_{total}}{E}$, where A_{total} is the surface area of the copper block which is covered by the

Teflon sleeves.

Hence, the heat flux uncertainty is

$$\frac{dq^{''}}{q^{''}} = \frac{dE}{E} + \frac{dA}{A} + \frac{q_{loss}^{''} A_{total}}{E} \qquad (C.10)$$

Table C.1 shows the uncertainties of heat flux for the surfaces under different experimental conditions. It can be found that the heat flux uncertainty ranges from 3.26% for the high heat flux value to 37.55% for the low heat flux value.

Table C.1 Heat flux uncertainty for different surfaces.

Surface Type	Bulk Liquid Condition	Heat Flux	Non-boiling Immersion Time (Hour)	Voltage (V)	Uncertainty
SSS	5 K Subcooled	Increased	72	20.6	0.2119694
		Increased	72	120.7	0.0579482
		Decreased	72	120.7	0.0579482
		Decreased	72	20.8	0.2789861
EDS	5 K Subcooled	Increased	72	20.3	0.218067
		Increased	72	120.3	0.0426307
		Decreased	72	120.3	0.0426307
		Decreased	72	20.5	0.1210789
HFS	5 K Subcooled	Increased	72	20.8	0.1945056
		Increased	72	120.2	0.0338765
		Decreased	72	120.2	0.0338765
		Decreased	72	20.7	0.1281979
SSS	Saturated	Increased	72	20.5	0.1502643
		Increased	72	120.2	0.0569913
		Decreased	72	120.2	0.0569913
		Decreased	72	20.5	**0.3755165**
EDS	Saturated	Increased	72	20.7	0.142856
		Increased	72	120.3	0.0426427
		Decreased	72	120.3	0.0426427
		Decreased	72	20.8	0.1141195
HFS	Saturated	Increased	72	20.8	0.1741235
		Increased	72	121	**0.0326491**
		Decreased	72	121	0.0326491
		Decreased	72	20.8	0.1002312
HFS	5 K Subcooled	Increased	48	20.7	0.214255
		Increased	48	120.8	0.0344422
		Decreased	48	120.8	0.0344422
		Decreased	48	20.3	0.1319857
HFS	5 K Subcooled	Increased	24	20.3	0.2124147
		Increased	24	120.8	0.0343037
		Decreased	24	120.8	0.0343343
		Decreased	24	20.3	0.1366736
HFS	5 K Subcooled	Increased	0	20.9	0.2108578
		Increased	0	120.4	0.0345028
		Decreased	0	120.4	0.0345028
		Decreased	0	20.3	0.1414794

BIBLIOGRAPHY

BIBLIOGRAPHY

1. Aitcheson, N. L. 2003. New surfaces for the control of boiling heat transfer: site formation at incipience. M.S. Thesis, Michigan State University.

2. Andrianov, A. B., Borzenko, V. I., and Malyshenko, S. P. 1999. Elementary processes at boiling on the surfaces with porous coatings. Russian Journal of Engineering Thermophysics, 9(1-2), pp. 51-67.

3. Bajorek, S. M. 1988. An experimental and theoretical investigation of multicomponent pool boiling on smooth and finned surfaces. Ph. D. Dissertation, Michigan State University.

4. Bankoff, S. G. 1959. The prediction of surface temperature of incipient boiling. Chemical Engineering Progress Symposium Series, 55, No. 29, pp.87-94.

5. Benjamin, J. E. and Westwater, J. W. 1961. Bubble growth in nucleate boiling in a binary mixture. International Development of Heat Transfer, pp. 212-218.

6. Berenson, P. J. 1960. Transition boiling heat transfer from a horizontal surface. Sc. D. Dissertation., Massachusetts Institute of Technology.

7. Berenson, P. J. 1962. Experiments on pool boiling heat transfer. International Journal of Heat and Mass Transfer, 5, pp. 985-999.

8. Bergles, A. E. and Chyu, M. C. 1982. Characteristics of nucleate pool boiling from porous metallic coatings, ASME Journal of Heat Transfer, 104, pp. 279-285.

9. Chang, J. Y. and You, S. M. 1997. Boiling heat transfer phenomena from micro-porous and porous surfaces in saturated FC-72. International Journal of Heat and Mass Transfer, 40 (18), pp. 4437-4447.

10. Chien, L. and Webb, R. L. 1998. A parametric study of nucleate boiling on structured surfaces. Part I: Effect of tunnel dimensions. ASME Journal of Heat Transfer, 120, pp. 1042-1048.

11. Chien, L. and Webb, R. L. 1998. A parametric study of nucleate boiling on structured surfaces. Part II: Effect of pore diameter and pore pitch. ASME Journal of Heat Transfer, 120, pp. 1049-1054.

75

12. Chien, L. and Webb, R. L. 1998. Measurement of bubble dynamics on an enhanced boiling surface. Experimental Thermal and Fluid Science, **16**, pp. 177-186.

13. Chien, L. and Webb, R. L. 2001. Effect of geometry and fluid property parameters on performance of tunnel and pore enhanced boiling surfaces. Experimental Thermal and Fluid Science, **8**, pp. 329-339.

14. Cieslinski, J. T. 2002. Nucleate pool boiling on porous metallic coatings. Experimental Thermal and Fluid Science, **25**, pp. 557–564.

15. Clark, H. B., Strengewater, P. S. and Westwater, J. W. 1959. Active sites for nucleate boiling. Chemical Engineering Progress Symposium Series, **55** (29), pp. 103-110.

16. Corty, C. and Foust, A. S. 1955. Surface variables in nucleate boiling. Chemical Engineering Progress Symposium Series, **51**, No.16, 1-12.

17. Demiray, F. and Kim, J. 2004. Microscale heat transfer measurements during pool boiling of FC-72: effect of subcooling. International Journal of Heat and Mass Transfer, **47**, pp. 3257-3268.

18. Griffith, P. and Wallis, J. D. 1960. The role of surface conditions in nucleate boiling. Chemical Engineering Progress Symposium Series, **56**, No.49, pp. 49-63.

19. Hsu, Y. Y. and Graham, R. W. 1976. Transport processes in boiling and two-phase system. Washington, D.C.: Hemisphere.

20. Hui, T. O. and Thome, J. R. 1985. A study of binary mixture boiling: Boiling site density and subcooled heat transfer. International Journal of Heat and Mass Transfer, **28**, pp.919-928.

21. Incropera, F. P. and DeWitt, D. P. 1981. Fundamentals of heat transfer. John Wiley & Sons.

22. Jiang, Y.Y., Wang, W.C., Wang, D. and Wang, B.X. 2001. Boiling heat transfer on machined porous surfaces with structural optimization. International Journal of Heat and Mass Transfer, **44**, 443-456,

23. Kedzierski, M. A. 1995. Calorimetric and visual measurements of R123 pool boiling on four enhanced surfaces. NISTIR 5732, U.S. Department of Energy, Washington, DC.

24. Kim, J. H., Rainey, K. N., You, S. M. and Pak, J. Y. 2002. Mechanism of nucleate boiling heat transfer enhancement from microporous surfaces in saturated FC-72. ASME Journal of Heat Transfer, **124**, pp. 500-506.

25. Kurihara, H. M. and Meyers, J. E. 1960. The effects of superheat and surface roughness on boiling coefficients. AIChE J., **6**(1), pp. 83-91.

26. Leontiev, A. I., Lloyd, J. R., Malyshenko, S. P., Borzenko, V. I., Dunikov, D. O. Eronin, A. A. and Nazarova, O. V. 2003. New effects in interfacial heat and mass transfer of boiling and evaporation in micro-scale porous materials. 2003 ASME IMECE Proceedings, Washington D.C., November 2003.

27. Lloyd, J. R. 1971. Laminar, transition, and turbulent natural convection adjacent to vertical and upward-facing inclined surfaces. Ph. D. Thesis, University of Minnesota.

28. Marto, P. J. and Lapere, Lt. V. J. 1982. Pool boiling heat transfer from enhanced surfaces to dielectric fluids, ASME Journal of Heat Transfer, **104**, pp. 292-299.

29. Miller, J. W., Gebhart, B. and Wright, N. T. 1990. Effects of boiling history on a microconfigured surface in a dielectric liquid. International Communications of Heat and Mass Transfer, **17**, pp. 389-398.

30. Milton, R. M. 1968. Heat exchange system. U.S. Patent 3,384,154. May 2.

31. Myers, J. E. and Katza, D. L. 1953. Boiling coefficients outside horizontal tubes. Chemical Engineering Progress Symposium Series, **49**, No.5, pp. 107-114.

32. Nakayama, W., Daikoku, T. and Nakajima, T. 1982. Effects of pore diameters and system pressure on saturated pool nucleate boiling heat transfer from porous surfaces. ASME Journal of Heat Transfer, **104**, pp. 286-291.

33. Ngai, S., Lloyd, J. R., Leontiev, A. I. and Malyshenko S. P. 2004. Creation of nano-scaled surface structure for the enhancement of boiling heat transfer. 2004 ASME IMECE Proceedings, Anaheim, California, November 2004.

34. Rainey, K. N., You, S. M. and Lee, S. 2003. Effect of pressure, subcooling, and dissolved gas on pool boiling heat transfer from microporous surfaces in FC-72. ASME Journal of Heat Transfer, **125**, pp. 75-83.

35. Ramaswamy, C., Joshi, Y., Nakayama, W. and Johnson, W. B. 2003. Effects of varying geometrical parameters on boiling from microfabricated enhanced structures. ASME Journal of Heat Transfer, **125**, pp. 103-109.

36. Ronsenow, W. M. 1982. Pool boiling. Handbook of Multiphase Systems, McGraw-Hill-Hemisphere, New York.

37. Shakir, S. 1987. Boiling Incipience and Heat Transfer on Smooth and Enhanced Surfaces. Ph. D. Dissertation, Michigan State University.

38. Shi, M.H., Ma, J. and Wang, B.X. 1993. Analysis on hysteresis in nucleate pool boiling heat transfer. International Journal of Heat and Mass Transfer, **36** (18), pp. 4461-4466.

39. Snyder, T. J., Chung, J. N. and Schneider, J. B. 1998. Competing effects of dielectrophoresis and buoyancy on nucleate boiling and an analogy with variable gravity boiling results. ASME Journal of Heat Transfer, **120**, pp. 371-379.

40. Still, W. J. 1929. Heat transmitting tube. U. S. Patent 1,716,743, June 11.

41. Tehver, J., Sui, H. and Temkina, V. 1992. Heat transfer and hysteresis phenomena in boiling on porous plasma-sprayed surface. Experimental Thermal and Fluid Science, **5**. pp.714-727.

42. Thome, J. R. 1990. Enhanced Boiling Heat Transfer. Hemisphere Publishing Corp.

43. Thome, J. R. 1992. Mechanisms of enhanced nucleate pool boiling. Proceedings of the Engineering Foundation Conference on Pool and External Flow Boiling, ASME, New York, pp. 337-343.

44. Vorob'ev, V.S. and Malyshenko, S.P. 2002. Nucleus formation in polarized dielectric media. Experimental Thermal and Fluid Science, **26**, pp. 833-839.

45. Webber, W. O. 1960. Under fouling conditions-Finned tubes can save money. Chemical Engineering, March, pp. 149-152.

46. Zhang, H. J., Li, L. J. and Tong, Q. M.1999. Boiling heat transfer from mechanically fabricated porous tubes at atmospheric and super atmospheric pressures. Heat Transfer-Asian Research, **28** (8), pp. 640-648.

47. <u>3M Material Safety Data Sheet FC-72 Fluorinert Brand Electronic Liquid</u>. 09/05/2002.

1
2